The charm contribution into the proton structure function in DIS at the HERA *ep*-collider

A.V.Berezhnoy, A.K.Likhoded

Abstract

In the framework of perturbative QCD and a model for the production of charmed hadrons the structure function F_2^c is calculated and compared with the experimental data of H1 and ZEUS Collaborations. We show that the spectator mechanism of the D^*-meson production independent of a hadronic remnant is valid at $p_T > 10$ GeV, only. We find that the evolution of $F_2^c(x, Q^2)$ versus the virtuality Q^2 can be neglected in the kinematic region of HERA.

1 Introduction

As well known, the DIS data in a broad kinematic region can be precisely described by a set of universal partonic distributions obeyed equations of the DGLAP-evolution [1] at large virtualities Q^2. Some difficulties appear when one tries to consider the heavy quark contribution into the function F_2^c in the DGALP-technique. The problem is caused by an accurate account of the kinematic region $Q^2 \sim 4m_q^2$, where, on one hand, we deal with high virtualities providing the applicability of pQCD, and, on the other hand, the mass effects should be appropriately treated and the heavy quarks cannot be considered as massless. Some attempts to take into account the heavy quarks contribution near the threshold and to match this contribution with the general DGLAP equations at large $Q^2 \gg 4m_q^2$ are presented in [2, 3]. In this work we consider c-quark production by making use of the notations in [2], where the attempt to match two different approaches for large Q^2 and $Q^2 \sim 4m_c^2$ was done.

The c-quark contribution into the structure function in the deep inelastic scattering can be obtained by convoluting the partonic distribution with the coefficient functions:

$$\begin{aligned}\frac{1}{x}F_2^c(x,Q^2) &= C_g(Q^2,\mu^2)\otimes f_g(\mu^2)[x] + \\ &+C_c(Q^2,\mu^2)\otimes f_c(\mu^2)[x] + \\ &+C_q(Q^2,\mu^2)\otimes f_q(\mu^2)[x], \end{aligned} \quad (1)$$

where f_i denote the partonic densities in the proton, the symbol $\otimes$ corresponds to the convolution over the variable x:

$$a\otimes b[x] = \int_x^1 \frac{dz}{z}a(z)b\left(\frac{x}{z}\right).$$

At small $\mu^2 < \mu_c^2$ the charm contents is $f_c(x,\mu^2) = 0$, and the structure function F_c^2 is completely described by the photon-gluon fusion $\gamma^* g \to c\bar{c}$, that gives $C_g(Q^2,\mu^2)\otimes f_g(\mu^2)$.

process $\gamma^* q \to c\bar{c}q$ is usually not taken into account because its contribution is suppressed by the additional power of α_s, however below we show that this process can play an essential role in the region of moderate p_T and Q^2.

In addition to the problem of matching the different approaches in the kinematic regions of $Q^2 \sim m_c^2$ and $Q^2 \gg 4m_c^2$, another important problem is connected to the comparison of theoretical predictions with the experimental data. So, F_c^2 is reconstructed in the ZEUS and H1 experiments [4] over the $D^{*\pm}$-meson production data obtained in two decay modes: $D^* \to K2\pi$, $D^* \to K4\pi$. The D^*-meson production cross section is measured in the restricted kinematic region: at ZEUS one puts $1 < Q^2 < 600$ GeV^2, $|\eta(D^*)| < 1.5$, $1.5 < p(D^*) < 15$ GeV, $0.02 < y < 0.7$, while the H1 Collaboration uses the similar kinematic region: $1 < Q^2 < 100$ GeV, $|\eta(D^*)| < 1.5$, $1.5 < p_T(D^*) < 10$ GeV, $0.05 < y < 0.7$. The cross section in the whole kinematic region is reconstructed under some model assumptions of charm production. One can conclude that the really measured quantities are the spectra of the charmed mesons in the restricted kinematic region, but the c-quark ones. That is why one has to define a procedure of the charmed quark hadronization in order to compare the calculated function $F_2^c(Q^2, x)$ with the experiment.

A procedure commonly used is based on the factorization theorem applied for the momentum spectrum of D^*-meson:

$$\frac{d\sigma_{D^*}}{dp_T} = \frac{d\sigma_c}{dk_T} \otimes D(z), \tag{2}$$

where $D(z)$ is the fragmentation function of $c \to D^*$, and $z = P_T/k_T$. The form of $D(z)$ is given by some kind of phenomenological anzätze [5]. Equation (2) should be a good approximation at large p_T and k_T, where the factorization theorem is valid. This theorem cannot be applied to the whole kinematic region since this could generate essential errors in the relation between the D^*-meson and c-quark spectra. The drawback of (2) is clearly seen in the H1 and ZEUS data: there is a visible excess of events in the region of pseudorapidity distribution towards the fragmentation of proton-beam. One can see the same features in the distribution over the variable $z_{D^*} = (Pp_{D^*})/(Pq)$, where P, p_{D^*}, q are four-momenta of the proton, D^*-meson and virtual photon, correspondingly. The discrepancy between next-to-leading-order (NLO) QCD prediction under the hadronization mechanism of (2) and the experimental data is more essential at large η_{D^*} and z_{D^*}.

Usually one tries to improve the data description by using some additional model assumptions incorporated in Monte-Carlo codes of event generator [4].

2 The charm production model

We will discuss the model where the attempt to take into account the hadronization from the very beginning is done. Let us consider the all pQCD $O(\alpha\alpha_s^3)$-diagrams, describing the perturbative production of the $c\bar{q}$-pair with the quantum numbers of the appropriate charm mesons.

$\bar{c}+q$ (see equation (1)). One needs the additional parameter $\langle O\rangle$ to take into account the contribution by the simultaneous production of c - and q-quarks. This parameter describes the fusion of c-quark and its light co-mover $\bar{q}$ into $(c\bar{q})$-system, and that is proportional to the D^*-meson wave function squared. This parameter can be extracted from the experimentally known value of the fragmentation probability W of $c \to D^*$ at large transverse momenta, $W = 0.23$ [6].

The $(c\bar{q})$-system can be in two color states: octet or singlet. In our previous analysis of the data on the charm photoproduction and electroproduction [7] we considered the production of color octet and color singlet states independently. So, we used two fusion parameters: $\langle O_{(1)}\rangle$ and $\langle O_{(8)}\rangle$, correspondingly. The ratio of these values is close to unit. At small p_T the color-singlet contribution into the cross section as well as the color-octet one behave as $1/p_T^6$, and they are approximately equal to each other. At large p_T both contributions behave like $(1/p_T^4)$, and the singlet term is dominant. The color-singlet dominance takes place due to the color-coefficient ratio. The both contributions at large p_T come to the fragmentation regime. In this regime the octet and singlet have a similar behavior, and the production process can be characterized by the only parameter:

$$\langle O^{\rm eff}\rangle = \langle O_{(1)}\rangle + \frac{1}{8}\langle O_{(8)}\rangle$$

. A more detail description of the model is represented in the Appendix.

One of essential features of this model consists of obeying the factorization theorem at large transverse momenta. In other words, at large p_T the formula of (2) describes the process with a good approximation, and the process looks like a fragmentation. At small momenta the fragmentation form of the charm production is strongly broken by additional terms $\sim 1/p_T^6$ in contrast to the fragmentation term, which behaves like $1/p_T^4$ as follows from (2).

One can see from Fig. 2 how the factorization theorem works at large p_T for both the singlet contribution and the octet one. The contributions of complete diagram-set (Fig. 1) in comparison with the contribution of the fragmentation diagram one (as in (2)) are presented in the figure for both the singlet and octet.

The calculations have been done at rather large value of $s_{\gamma g} = (p_\gamma + p_g)^2 = 200^2 \mathrm{GeV}^2$ in order to reach the factorization regime (2). One can see from the figure that there is the region of p_T, where the fragmentation mechanism is not valid, and the contribution of perturbative recombination is dominant. The presence of the recombination contribution is due to the gauge invariance of QCD. The p_T-dependence of this contribution has the additional factor $1/p_T^2$, that is why the recombination vanishes at large p_T, and the D^*-meson production is described by the factorization formula of (2).

3 The D^*-meson electroproduction

As was mentioned above, the model under consideration has been used to describe the charm photoproduction data of ZEUS Collaboration [8]. The fragmentation probability $W(c \to D^*)$

mass: $\mu_F = m_{D^*}$. The light quark mass equals $m_{\bar{q}} = 0.3$ GeV, and the c -quark mass equals $m_c = 1.5$ GeV.

The factorization probability $W(c \to D^*) = 0.23$, while $\langle O^{\rm eff} \rangle = 0.25$ GeV^3. The ratio between the octet and singlet operators has been chosen equal to $\langle O_{(8)} \rangle / \langle O_{(1)} \rangle = 1.3$. It is worth to mention that taking into account the color-octet contribution essentially improves the description of the experimental data, especially, in the description of the pseudorapidity distribution. In this distribution the octet enforces the production into the forward semisphere (toward the direction of the initial proton) and improves the data description in comparison with the NLO prediction [7].

The calculations of cross section for the D^*-meson electroproduction have been made by practically the same manner as for the photoproduction. All we need is to replace the density-matrix of real photon by the density-matrix of virtual photon. So, after averaging over the photon and electron polarizations the D^*-meson elecroproduction amplitude squared has the following from:

$$|A|^2 = \sum_{ij} \frac{k_1^i k_2^j + k_1^j k_2^i - \frac{Q^2}{2} g^{ij}}{Q^4} M_i M_j^*, \tag{3}$$

where $|A|^2$ is the D^*-meson electroproduction amplitude squared, M_i is the D^*-meson photoproduction amplitude (i is the Lorentz index of the photon polarization), $k_1$and k_2 are the initial and final positron momenta, and $Q^2 = -(k_1 - k_2)^2$. The calculation results are presented in Figs. 3 and 4 in comparison with the experimental data of the H1 and ZEUS Collaborations, correspondingly. The calculations have been done with the same cuts as in the appropriate experiments. The singlet contribution is plotted by the dashed curve, the octet contribution is plotted by the dotted curve; the solid curve corresponds to the sum of these contributions.

We have used two values of the scale for the running coupling constant of QCD in our calculations: $\mu_R = \sqrt{m_{D^*}^2 + Q^2}$ (upper curve) and $\mu_R = \sqrt{4m_{D^*}^2 + Q^2}$ (lower curve) and the scale value $\mu_F = \sqrt{m_{D^*}^2 + Q^2}$ for the CTEQ4 parameterization of the structure function. As one can see from the figures the model prediction is in agreement with the experimental data. Such the good description is achieved due to taking into account the octet contribution. This contribution improves the distributions over the pseudorapidity $\eta(D^*)$ (as in the photoproduction); over the variable $z(D^*)$ measured in the H1 experiment, and over the variable $x(D^*) = |\vec{p}^*(D^*)|/W$ measured in the ZEUS experiment ($\vec{p}^*(D^*)$ is the D^*-meson 3-momentum in the c.m.s. of initial virtual photon and proton). It is worth to mention another feature of the octet contribution. It is essential at small p_T and becomes negligible at large ones, where it is suppressed by the color-factor 1/8.

Thus, in the framework of the model under consideration we have achieved a good description for the ZEUS charm-photoproduction data [8] as well as for the charm-electroproduction data of H1 and ZEUS Collaborations [4]. This circumstance allows us to suppose that the extrapolation of the experimental data into the total kinematic region with the help of our model is rather reliable. It means, that we can calculate the total cross section production and, therefore, extract F_2^c.

The charm contribution F_2^c into the structure function F_2 is defined by the doubly differential cross-section of the charm-production as follows:

$$\frac{d^2\sigma^c(Q^2,x)}{dxdQ^2} = \frac{2\pi\alpha_s^2}{\alpha Q^4}\left\{\left[1+(1-y)^2\right]F_2^c - y^2F_L^c(Q^2,x)\right\} \tag{4}$$

Generally one neglects the contribution of the longitudinal component F_L because of its suppression. As was mentioned in the Introduction, F_2^c is reconstructed on the base of the experimental data for the D^*-meson production in the experimentally available kinematic region. The observed production cross section is extrapolated into the total kinematic region in the framework of some model. Thus, it is clear that the F_2^c value depends on a model. In the framework of our model we have an opportunity to calculate the cross section in the total kinematic region, determine F_2^c, and compare it with the results of ZEUS and H1 Collaborations.

The experimental dependence of F_2^c on x for different Q^2 values is shown in Fig. 5 by dots (the H1 Collaboration). These data were extracted by the extrapolation of the experimentally observed cross section into the total kinematic region on the base of NLO calculations and Monte-Carlo programs taking into account the hadronization.

The curves in this figure correspond to our model predictions. F_2^c has been calculated according to formula (4). The falls on the distribution tails appear because of the phase-space borders for the given value of the ep -interaction energy and chosen values for the quark masses.

The ZEUS experimental data on F_2^c are shown in Fig. 6 in comparison with the predictions of our model .

5 The perturbative recombination

One can see that the operator expansion of (1) contains not only the term interpreted as photon-gluon production of charm, but also that of describing the photon-quark production of charm. Generally one neglects this term due to the additional factor of α_s.

The diagrams, which correspond to the photon-quark term in our approach, are shown in Fig. 7. For such kind of diagrams the only difference between the color-octet production cross section and the color-singlet one is due to the overall color factor of 1/8. That is why we can restrict ourselves by considering the singlet production, only.

The recent analysis demonstrates that at large transverse momenta p_T the photon-quark production contribution is suppressed by an additional factor $1/p_T^2$. At small p_T the suppression is absent, and the differential cross section of the $(\bar{c}q)$ pair production at the angle $\Theta = 0$ (toward the direction of initial quark q) has a large numerical coefficient in comparison with the c-quark production in the $g\gamma$-interaction [9]:

$$\frac{d\hat{\sigma}(\gamma + q \to (\bar{c}q) + c)}{d\hat{\sigma}(\gamma + g \to \bar{c}c)} \simeq \frac{256\pi}{81}\alpha_s. \tag{5}$$

Thus, the smallness of α_s in the photon-quark production cross section is compensated by large numerical coefficient. To the same moment, the production at the angle $\Theta = \pi$ is

In paper [7] the $c\bar{q}$-pair production cross section in the interaction of the photon and valence quark from the initial proton has been calculated to evaluate the D^+/D^- and $D^0/\bar{D}^0$ asymmetries. The predicted value of asymmetry in the kinematic regions researched by the ZEUS and H1 Collaborations is about 2-3%, that is in the same order of magnitude as experimental errors. At low energies of γp-interactions, the role of the photon-quark production becomes essential and this contribution yields the asymmetry prediction which is in a good agreement with the experimental data [9]. If the production asymmetry is due to the perturbative recombination indeed, then the asymmetry decreases with the p_T increase, because the perturbative recombination has the additional $1/p_T^2$ factor in comparison with the leading contributions. On the other hand, if the asymmetry is due to the interaction between the c-quark and the valence quark from the initial hadron, then the interaction between the c-quark and the light quark from the initial hadron sea exists. Such the contribution has been calculated in the framework of our model, and it surprisingly looks like the octet contribution in the distribution shape as well as in the absolute value. It is worth to mention that the quark-photon contribution does not contain an additional normalization factor, which the octet one contains. In Fig. 7 both the octet and quark-photon contributions into the D^*-meson production are presented for the kinematic region investigated by the H1 Collaboration. One can see that the distributions over $\log_{10}(x)$ and p_T are practically the same for the whole investigated range. One can see the only small difference in the normalization. The Q^2-distributions at $Q^2 < 10$ GeV^2 have practically the qualitatively similar behavior, too. The differences between the distributions over W, $\eta(D^*)$ and $z(D^*)$ are more essential for the production mechanisms compared. However, these distributions have qualitatively analogous behavior. The singlet $c\bar{q}$-pair yield in γg- and $\gamma\bar{q}$-interactions is presented in Fig. 8 for the kinematic conditions of H1 experiment. It is clear from this figure that at not very large Q^2 the sum of the γg- and $\gamma\bar{q}$-contributions into the singlet describes the data so good as the sum of γg-contributions into the singlet and octet.

Therefore, the singlet $c\bar{q}$-pair production mechanism is enough to describe the charm photoproduction and electroproduction data in the HERA experiments. The photon-gluon contribution as well as the quark-photon one play essential role for the singlet $c\bar{q}$-pair production at the HERA interaction energy. The serious arguments to take into account the sea quark contribution into the charm production was presented in paper [9], where the charm production asymmetry has been successfully described in the framework of perturbative recombination in the E687 and E691 experiments.

6 Conclusions

The model under consideration is based, at first, on the heavy-quark production in the perturbative theory, and second, it uses the nonperturbative model of quarks fusion into the hadron. This model allows us to describe the existing data on charm photoproduction and electroproduction in the total kinematic region.

Let us itemize the main features of the model predictions:

mentum spectrum of $c\bar{q}$-pair is calculated by convolving the heavy quark spectrum with the fragmentation function.

2. In the region of small transverse momenta and small Q^2 the main contribution into the inclusive spectrum is due to the recombination diagrams, that depends on p_T as $1/p_T^6$, in contrast to the fragmentation ones, which depend on p_T as $1/p_T^4$. The contributions of $g\gamma$- and $q\gamma$-interactions into the charm production are comparable.

3. It is not necessary to include the term $C_c \otimes c$ of F_2^c (the second term in expansion(1)) into the data description at the HERA energies. According to the paper [2] the term $C_c \otimes c$ becomes essential at large Q^2.

Therefore our main conclusion is formulated as follows: the spectator character of the D^*-meson production, which is independent of the flavor of the initial hadron remnant, becomes dominant at $p_T > 10$ GeV. At small transverse momenta the essential part of the cross section is due to the interaction with the initial hadron remnant. The interaction with the valence quark of the remnant explains the experimentally observed flavor asymmetry in the charm yield.

7 Acknowledgments

We thank V. Kiselev for useful discussions. This work was in part supported by the Russian foundation for basic research, grants 01-02-99315, 01-02-16585 and 00-15-96645, the Russian Ministry on the education, grant E00-3.3-62.

Appendix

A. The hard production of four quarks in the photon-gluon subprocess

As was mentioned above, in the model under consideration one supposes that the both valence quarks, the heavy and light ones, are produced in the hard process.

In the framework of the tree level approach to the subprocess $g(p_g) + \gamma(p_\gamma) \to c(q_c) + \bar{c}(q_{\bar{c}}) + d(q_q) + \bar{q}(q_{\bar{q}})$ 24 Feynman diagrams contribute (see Fig. 1; he bold line corresponds to the c-quark, the thin line corresponds to the d-quark). In this paper the amplitude calculation has been done by straightforward multiplying of γ-matrices, spinors and polarization vectors.

Let us introduce the following notations:

$$\begin{gathered} q_c^2 = q_{\bar{c}}^2 = m_c^2, \qquad q_q^2 = q_{\bar{q}}^2 = m_q^2, \\ q_{c\bar{c}} = -q_c - q_{\bar{c}}, \qquad q_{q\bar{q}} = -q_q - q_{\bar{q}}, \qquad p_{g\gamma} = p_g + p_\gamma, \\ k_{g,c\bar{c}} = p_g + q_{c\bar{c}}, \qquad k_{g,q\bar{q}} = p_g + q_{q\bar{q}}. \end{gathered} \tag{6}$$

$$
\begin{aligned}
\Gamma^{\mu}(p_a,p_b,\epsilon_a,\epsilon_b) &= -\Big((2p_a+p_b)\cdot\epsilon_b\Big)\epsilon_a^{\mu}+(p_a-p_b)^{\mu}\Big(\epsilon_a\cdot\epsilon_b\Big)\\
&\quad+\Big((2p_b+p_a)\cdot\epsilon_a\Big)\epsilon_b^{\mu},\\
\Gamma'^{\mu}(p_a,p_b,\epsilon_a,\epsilon_b) &= \Gamma^{\mu}(p_a,p_b,\epsilon_a,\epsilon_b)/(p_a+p_b)^2. \qquad (7)
\end{aligned}
$$

The bi-quark currents are defined as follows:

$$
J^{\mu}_{c\bar{c}}=\frac{\bar{u}(q_c)\gamma^{\mu}v(q_{\bar{c}})}{q^2_{c\bar{c}}},\qquad\qquad J^{\mu}_{q\bar{q}}=\frac{\bar{u}(q_q)\gamma^{\mu}v(q_{\bar{q}})}{q^2_{q\bar{q}}}. \qquad (8)
$$

Also we need to define the auxiliary spinors

$$
\begin{aligned}
\bar{u}_{c(q)g(\gamma)}=\bar{u}(q_{c(q)})\hat{\epsilon}_{g(\gamma)}\frac{(\hat{q}_{c(q)}-\hat{p}_{g(\gamma)}+m_{c(q)})}{(q_{c(q)}-p_{g(\gamma)})^2-m^2_{c(q)}},&\qquad v_{\bar{c}(\bar{q})g(\gamma)}=\frac{(\hat{p}_{g(\gamma)}-\hat{q}_{\bar{c}(\bar{q})}+m_{\bar{c}(\bar{q})})}{(p_{g(\gamma)}-q_{\bar{c}(\bar{q})})^2-m^2_{\bar{c}(\bar{q})})}\hat{\epsilon}_{g(\gamma)}v(q_i),\\
\bar{u}_{c,q\bar{q}}=\frac{\bar{u}(q_c)\hat{J}_{q\bar{q}}(\hat{q}_c-\hat{q}_{q\bar{q}}+m_c)}{(q_c-q_{q\bar{q}})^2-m^2_c},&\qquad \bar{u}_{d,c\bar{c}}=\frac{\bar{u}(q_q)\hat{J}_{c\bar{c}}(\hat{q}_q-\hat{q}_{c\bar{c}}+m_q)}{(q_q-q_{c\bar{c}})^2-m^2_q},\\
v_{\bar{c},q\bar{q}}=\frac{(\hat{q}_{q\bar{q}}-\hat{q}_{\bar{c}}+m_c)\hat{J}_{q\bar{q}}v(q_{\bar{c}})}{(q_{q\bar{q}}-q_{\bar{c}})^2-m^2_c},&\qquad v_{\bar{q},c\bar{c}}=\frac{(\hat{q}_{c\bar{c}}-\hat{q}_{\bar{q}}+m_q)\hat{J}_{c\bar{c}}v(q_{\bar{q}})}{(q_{c\bar{c}}-q_{\bar{q}})^2-m^2_q}, \qquad (9)
\end{aligned}
$$

where ϵ_g and ϵ_γ are the polarization vectors of the gluon and photon, correspondingly. The matrix element squared is summed over the following ortonormalized states of gluon:

$$
\epsilon'=(0,1,0,0),\quad \epsilon''=(0,0,1,0).
$$

It is worth to mention that $\epsilon'^2=\epsilon''^2=-1$, and $p\cdot\epsilon=0$, where p is gluon momentum.

In the case of deep inelastic production the photon is off mass shell, and one need to replace the matrix $\hat{\epsilon}_2$ in (9) by the matrix γ^i. Thus the matrix element will have a free Lorentz index for convolving with the photon density in accordance with formula (3).

We use the following index definitions:

the upper indices j_g designate the color state of gluon;

the low index i_c designates the color state of c-quark;

the low index $i_{\bar{c}}$ designates the color state of $\bar{c}$-quark;

the low index i_q designates the color state of d-quark;

the low index $i_{\bar{q}}$ designates the color state of $\bar{q}$-quark.

The contributions of the Feynman diagrams into the total amplitude can be written as follows (e_q and e_c are electric charges of the q- and c-quarks correspondingly; the color coefficients are put into the braces):

$$
\begin{aligned}
T_1 &= e_c\cdot\bar{u}(q_q)\hat{\Gamma}'(p_g,q_{c\bar{c}},\epsilon_g,J_{c\bar{c}})v_{\bar{q}\gamma}\cdot\{if^{n_1n_2j_g}t^{n_1}_{i_ci_{\bar{c}}}t^{n_2}_{i_di_{\bar{q}}}\}, &(10)\\
T_2 &= e_c\cdot\bar{u}_{q\gamma}\hat{\Gamma}'(p_g,q_{c\bar{c}},\epsilon_g,J_{c\bar{c}})v(q_{\bar{q}})\cdot\{if^{n_1n_2j_g}t^{n_1}_{i_ci_{\bar{c}}}t^{n_2}_{i_di_{\bar{q}}}\}, &(11)\\
T_3 &= e_q\cdot\bar{u}(q_c)\hat{\Gamma}'(p_g,q_{q\bar{q}},\epsilon_g,J_{q\bar{q}})v_{\bar{c}\gamma}\cdot\{if^{n_1n_2j_g}t^{n_1}_{i_di_{\bar{q}}}t^{n_2}_{i_ci_{\bar{c}}}\}, &(12)\\
T_4 &= e_q\cdot\bar{u}_{c\gamma}\hat{\Gamma}'(p_g,q_{q\bar{q}},\epsilon_g,J_{q\bar{q}})v(q_{\bar{c}})\cdot\{if^{n_1n_2j_g}t^{n_1}_{i_di_{\bar{q}}}t^{n_2}_{i_ci_{\bar{c}}}\}, &(13)\\
T_5 &= e_c\cdot\bar{u}_{cg}\gamma^{\alpha}v(q_{\bar{c}})\bar{u}(q_q)\gamma_{\alpha}v_{\bar{q}\gamma}/k^2_{g,c\bar{c}}\cdot\{t^{j_g}_{i_cl}t^{n}_{li_{\bar{c}}}t^{n}_{i_qi_{\bar{q}}}\}, &(14)
\end{aligned}
$$

$$T_8 = e_c \cdot \bar{u}(q_c)\gamma^\alpha v_{\bar{c}g}\bar{u}_{q\gamma}\gamma_\alpha v(q_{\bar{q}})/k^2_{g,c\bar{c}} \cdot \{t^n_{i_c l}t^{j_g}_{li_{\bar{c}}}t^n_{i_q i_{\bar{q}}}\}, \quad (17)$$

$$T_9 = e_q \cdot \bar{u}_{qg}\gamma^\alpha v(q_{\bar{q}})\bar{u}(q_c)\gamma_\alpha v_{\bar{c}\gamma}/k^2_{g,q\bar{q}} \cdot \{t^n_{i_c i_{\bar{c}}}t^{j_g}_{i_q l}t^n_{li_{\bar{q}}}\}, \quad (18)$$

$$T_{10} = e_q \cdot \bar{u}(q_q)\gamma^\alpha v_{\bar{q}g}\bar{u}(q_c)\gamma_\alpha v_{\bar{c}\gamma}/k^2_{g,q\bar{q}} \cdot \{t^n_{i_c i_{\bar{c}}}t^n_{i_q l}t^{j_g}_{li_{\bar{q}}}\}, \quad (19)$$

$$T_{11} = e_q \cdot \bar{u}_{qg}\gamma^\alpha v(q_{\bar{q}})\bar{u}_{c\gamma}\gamma_\alpha v(q_{\bar{c}})/k^2_{g,q\bar{q}} \cdot \{t^n_{i_c i_{\bar{c}}}t^{j_g}_{i_q l}t^n_{li_{\bar{q}}}\}, \quad (20)$$

$$T_{12} = e_q \cdot \bar{u}(q_q)\gamma^\alpha v_{\bar{q}g}\bar{u}_{c\gamma}\gamma_\alpha v(q_{\bar{c}})/k^2_{g,q\bar{q}} \cdot \{t^n_{i_c i_{\bar{c}}}t^n_{i_q l}t^{j_g}_{li_{\bar{q}}}\}, \quad (21)$$

$$T_{13} = e_q \cdot \bar{u}_{c,q\bar{q}}\hat{\epsilon}_g v_{\bar{c}\gamma} \cdot \{t^n_{i_c l}t^{j_g}_{li_{\bar{c}}}t^n_{i_q i_{\bar{q}}}\}, \quad (22)$$

$$T_{14} = e_q \cdot \bar{u}_{cg}\hat{J}_{q\bar{q}}v_{\bar{c}\gamma} \cdot \{t^{j_g}_{i_c l}t^n_{li_{\bar{c}}}t^n_{i_q i_{\bar{q}}}\}, \quad (23)$$

$$T_{15} = e_q \cdot \bar{u}_{cg}\hat{\epsilon}_\gamma v_{\bar{c},q\bar{q}} \cdot \{t^{j_g}_{i_c l}t^n_{li_{\bar{c}}}t^n_{i_q i_{\bar{q}}}\}, \quad (24)$$

$$T_{16} = e_c \cdot \bar{u}_{c,q\bar{q}}\hat{\epsilon}_\gamma v_{\bar{c}g} \cdot \{t^n_{i_c l}t^{j_g}_{li_{\bar{c}}}t^n_{i_q i_{\bar{q}}}\}, \quad (25)$$

$$T_{17} = e_q \cdot \bar{u}_{c\gamma}\hat{J}_{q\bar{q}}v_{\bar{c}g} \cdot \{t^n_{i_c l}t^{j_g}_{li_{\bar{c}}}t^n_{i_q i_{\bar{q}}}\}, \quad (26)$$

$$T_{18} = e_q \cdot \bar{u}_{c\gamma}\hat{\epsilon}_g v_{\bar{c},q\bar{q}} \cdot \{t^{j_g}_{i_c l}t^n_{li_{\bar{c}}}t^n_{i_q i_{\bar{q}}}\}, \quad (27)$$

$$T_{19} = e_c \cdot \bar{u}_{q,c\bar{c}}\hat{\epsilon}_g v_{\bar{q}\gamma} \cdot \{t^n_{i_q l}t^{j_g}_{li_{\bar{q}}}t^n_{i_c i_{\bar{c}}}\}, \quad (28)$$

$$T_{20} = e_c \cdot \bar{u}_{qg}\hat{J}_{c\bar{c}}v_{\bar{q}\gamma} \cdot \{t^{j_g}_{i_q l}t^n_{li_{\bar{q}}}t^n_{i_c i_{\bar{c}}}\}, \quad (29)$$

$$T_{21} = e_c \cdot \bar{u}_{qg}\hat{\epsilon}_\gamma v_{\bar{q},c\bar{c}} \cdot \{t^{j_g}_{i_q l}t^n_{li_{\bar{q}}}t^n_{i_c i_{\bar{c}}}\}, \quad (30)$$

$$T_{22} = e_q \cdot \bar{u}_{q,c\bar{c}}\hat{\epsilon}_\gamma v_{\bar{q}g} \cdot \{t^n_{i_q l}t^{j_g}_{li_{\bar{q}}}t^n_{i_c i_{\bar{c}}}\}, \quad (31)$$

$$T_{23} = e_c \cdot \bar{u}_{q\gamma}\hat{J}_{c\bar{c}}v_{\bar{q}g} \cdot \{t^n_{i_q l}t^{j_g}_{li_{\bar{q}}}t^n_{i_c i_{\bar{c}}}\}, \quad (32)$$

$$T_{24} = e_c \cdot \bar{u}_{q\gamma}\hat{\epsilon}_g v_{\bar{q},c\bar{c}} \cdot \{t^{j_g}_{i_q l}t^n_{li_{\bar{q}}}t^n_{i_c i_{\bar{c}}}\}, \quad (33)$$

The spinor states with the fixed spin projection on the axis z have been chosen in the capacity of two independent spinor states. In our calculations, the Dirac representation for the γ-matrices has been used. The spinor states can be written down as follows:

$$u(p,+) = \frac{1}{\sqrt{E+m}}\begin{pmatrix} E+m \\ 0 \\ p_z \\ p_x+ip_y \end{pmatrix},$$

$$u(p,-) = \frac{1}{\sqrt{E+m}}\begin{pmatrix} 0 \\ E+m \\ p_x-ip_y \\ -p_z \end{pmatrix},$$

$$v(p,+) = -\frac{1}{\sqrt{E+m}}\begin{pmatrix} p_z \\ p_x+ip_y \\ 0 \\ E+m \end{pmatrix},$$

$$v(p,-) = \frac{1}{\sqrt{E+m}}\begin{pmatrix} p_x-ip_y \\ p_z \\ 0 \\ E+m \end{pmatrix}. \quad (34)$$

$$\gamma^0 = \begin{pmatrix} 1 & 0 \\ 0 & -1 \end{pmatrix}, \qquad \vec{\gamma} = \begin{pmatrix} 0 & \vec{\sigma} \\ -\vec{\sigma} & 0 \end{pmatrix},$$

$$\vec{\sigma} = \{\sigma_x, \sigma_y, \sigma_z\} = \left\{ \begin{pmatrix} 0 & 1 \\ 1 & 0 \end{pmatrix}, \quad \begin{pmatrix} 0 & -i \\ i & 0 \end{pmatrix}, \quad \begin{pmatrix} 1 & 0 \\ 0 & -1 \end{pmatrix} \right\}$$

The Gell-Mann matrices have the form

$$\lambda^1 = \begin{pmatrix} 0 & 1 & 0 \\ 1 & 0 & 0 \\ 0 & 0 & 0 \end{pmatrix}, \qquad \lambda^2 = \begin{pmatrix} 0 & -i & 0 \\ i & 0 & 0 \\ 0 & 0 & 0 \end{pmatrix}, \qquad \lambda^3 = \begin{pmatrix} 1 & 0 & 0 \\ 0 & -1 & 0 \\ 0 & 0 & 0 \end{pmatrix},$$

$$\lambda^4 = \begin{pmatrix} 0 & 0 & 1 \\ 0 & 0 & 0 \\ 1 & 0 & 0 \end{pmatrix}, \qquad \lambda^5 = \begin{pmatrix} 0 & 0 & -i \\ 0 & 0 & 0 \\ i & 0 & 0 \end{pmatrix}, \qquad \lambda^6 = \begin{pmatrix} 0 & 0 & 0 \\ 0 & 0 & 1 \\ 0 & 1 & 0 \end{pmatrix},$$

$$\lambda^7 = \begin{pmatrix} 0 & 0 & 0 \\ 0 & 0 & -i \\ 0 & i & 0 \end{pmatrix}, \qquad \lambda^8 = \frac{1}{\sqrt{3}} \begin{pmatrix} 1 & 0 & 0 \\ 0 & 1 & 0 \\ 0 & 0 & -2 \end{pmatrix},$$

and the t-matrices have been chosen as $t^i = \frac{1}{2}\lambda^i$.

Let us remind of the antisymmetric constant f_{abc} values, which have been required for our calculations

$$f_{123} = 1,$$
$$f_{147} = -f_{156} = f_{246} = f_{257} = f_{345} = -f_{367} = \tfrac{1}{2},$$
$$f_{458} = f_{678} = \tfrac{\sqrt{3}}{2}.$$

B. The soft process of c- and $\bar{q}$-quark fusion into the $(c\bar{q})$-quarkonium

To describe the fusion of c- and $\bar{q}$-quarks into the $(c\bar{q})$-quarkonium we suppose that there are terms in the partonic distribution of D^*-meson, which correspond to the valence quarks. We also suppose that the c- and $\bar{q}$-quarks produced in the hard process transform into the valence quarks of the meson. The valence quark distributions in the system of infinite momentum have the following form:

$$f_c^v(x, p_\perp) = f_c(x, p_\perp) - f_{\bar{c}}(x, p_\perp),$$

$$f_{\bar{q}}^v(x, p_\perp) = f_{\bar{q}}(x, p_\perp) - f_q(x, p_\perp).$$

The averaged momentum fraction carried out by the valence quarks are

$$\langle x_c^v \rangle = \int d^2p_\perp dx x \cdot f_c^v(x, p_\perp) \approx \frac{m_c}{m_{D^*}}, \tag{35}$$

$$\langle x_{\bar{q}}^v \rangle = \int d^2p_\perp dx x \cdot f_{\bar{q}}^v(x, p_\perp) \approx \frac{\bar{\Lambda}}{m_{D^*}}, \tag{36}$$

$$\langle x_c^v \rangle + \langle x_{\bar{q}}^v \rangle \approx 1. \tag{37}$$

In our calculation we neglect the dispersion of the momentum fractions carried out by the quarks, or in other words, we consider (35,36,37) as absolutely precise equations. Also we suppose that the light quark mass is about $\bar{\Lambda}$.

In the doubly heavy quarkonium the quark pair is in the singlet state, because the octet one is suppressed by the third power of the relative velocity of quarks [10]. In the case of $(c\bar{q})$-quarkonium this suppression does not exist, and one has to take into account the both color states.

The operators $\langle O_{(1)} \rangle$ and $\langle O_{(8)} \rangle$ describing the hadronization of singlet and octet quark pairs into the meson are nonperturbative, because they include the interaction on the scale about $\Lambda_{\rm QCD}$. In the framework of nonrelativistic potential model these operators correspond to the wave functions squared at the origin: $\langle O_{(1,8)} \rangle|_{\rm NR} = |\Psi(0)|^2$. They are defined by

$$\langle O_{(1)} \rangle = \frac{1}{12 M_{D^*}} \left(-g^{\mu\nu} + \frac{p^\mu p^\nu}{M_{D^*}^2} \right) \times \langle D^*(p)|(\bar{c}\gamma_\mu q)(\bar{q}\gamma_\nu c)|D^*(p)\rangle, \tag{38}$$

$$\langle O_{(8)} \rangle = \frac{1}{8 M_{D^*}} \left(-g^{\mu\nu} + \frac{p^\mu p^\nu}{M_{D^*}^2} \right) \times \langle D^*(p)|(\bar{c}\gamma_\mu \lambda^a q)(\bar{q}\gamma_\nu \lambda^b c)|D^*(p)\rangle \frac{\delta^{ab}}{8}. \tag{39}$$

The probability $W(c \to D^*)$ of c-quark fragmentation into the D^*-meson in e^+e^--annihilation can be expressed through the operators $\langle O_{(1)} \rangle$ and $\langle O_{(8)} \rangle$ of our model

$$W(c \to D^*) = \int_0^1 D_{c \to D^*}(z) dz = \frac{\alpha_s^2(\mu_R) \langle O^{\rm eff}(\mu_R) \rangle}{m_q^3} I\left(\frac{m_q}{m_q + m_c} \right), \tag{40}$$

where $\langle O^{\rm eff}(\mu_R) \rangle = \langle O_{(1)} \rangle + \frac{1}{8} \langle O_{(8)} \rangle$, and

$$I(r) = \frac{8}{27} \left[\frac{24 + 109r - 126r^2 - 174r^3 - 89r^4}{15(1-r)^5} + \frac{r(7 - 4r - 3r^3 + 10r^3 + 2r^4)}{(1-r)^6} \ln r \right]. \tag{41}$$

References

[1] Y.L. Dokshitzer, JETP **73**, 1216 (1971);
V.N. Gribov, L.N. Lipatov, Sov. J. Nucl. Phys. **15**, 78 (1972);
G. Altarelli, G. Parisi, Nucl. Phys. B **126**, 298 (1977);
G. Altarelli, Phys. Rep. **81**, 1 (1982).

[2] J. C. Collins, A. D. Martin and M. G. Ryskin, Preprint hep-ph/9709440, in "Madrid 1997, Low x physics",134; J. C. Collins, A. D. Martin and M. G. Ryskin, Eur. Phys. J. C **2**, 287 (1998).

[3] J. Amundson *et al.*, Preprint hep-ph/0005221, JHEP, 0010 (2000); J. C. Collins and W. Tung, Nucl.Phys. B **278**, 934 (1986); F. I. Collins and W. Tung, Nucl.Phys. B **308**, 813 (1988); M. A. Aivazis, F. I. Collins and W. Tung, Phys.Rev. D **50**, 3085(1994); M. A. Aivazis

Chicago, IL, 1997"; R. S. Thorne and R. G. Roberts, Phys.Rev. D **57**, 6871(1998); M. Buza *et al.*, Eur.Phys.J. C **1**, 301(1998); M. Cacciari, M. Greco and P. Nason, JHEP **9805**, 007(1998); A. Chuvakin, J. Smith and W. L. van Neerven, Phys.Rev. D **61**, 096004(2000); A.V. Kisselev, V.A. Petrov and R.A. Ryutin, Preprint hep-ph/0109271

[4] ZEUS Collab. (J. Breitweg *et al.*), Eur.Phys.J. C **12**, 35 (2000); H1 Collab. (C. Adloff *et al.*), Preprint hep-ex/0108039, submitted to Phys.Lett.B.

[5] C. Peterson *et al.*, Phys.Rev. D **27**, 105 (1983); V. G. Kartvelishvili, A. K. Likhoded and V. A. Petrov, Phys.Lett. B **78**, 615 (1978).

[6] OPAL Collab. (K.Akerstaff *et al.*), Eur.Phys.J. C **1**, 439 (1998), L. Gladilin, Preprint hep-ph/9912064 , ALEPH Collab. (R. Barate *et al.*), Eur.Phys.J. C **16**, 597 (2000).

[7] A. V. Berezhnoy, V. V. Kiselev and A. K. Likhoded, Phys.Rev. D **62**, 074013 (2000), Phys. Atom. Nucl. **63**, 1595 (2000) [Yad. Fiz. **63**, 1682 (2000)], Preprint hep-ph/9901333.

[8] ZEUS Collab. (J. Breitweg *et al.*), Eur.Phys.J. C **6**, 67 (1999).

[9] E. Braaten, Y. Jia and T. Mehen, Preprint hep-ph/0108201.

[10] G. T. Bodwin, E. Braaten and G. P. Lepage, Phys.Rev. D **51**, 1125 (1995); T. Mannel and G. A. Shuler, Z.Phys. C **67**, 159 (1995); E. Braaten, S. Fleming and T. C. Yuan, Annu.Rev.Nucl. Part. Sci. **46**, 197 (1996); S.S. Gershtein, V.V. Kiselev, A.K. Likhoded, A.V. Tkabladze (Serpukhov, IHEP). IFVE-94-81, Jun 1994. 81pp. Published in Phys.Usp.**38**,1 (1995), Usp.Fiz.Nauk **165**, 3 (1995), Preprint hep-ph/9504319.

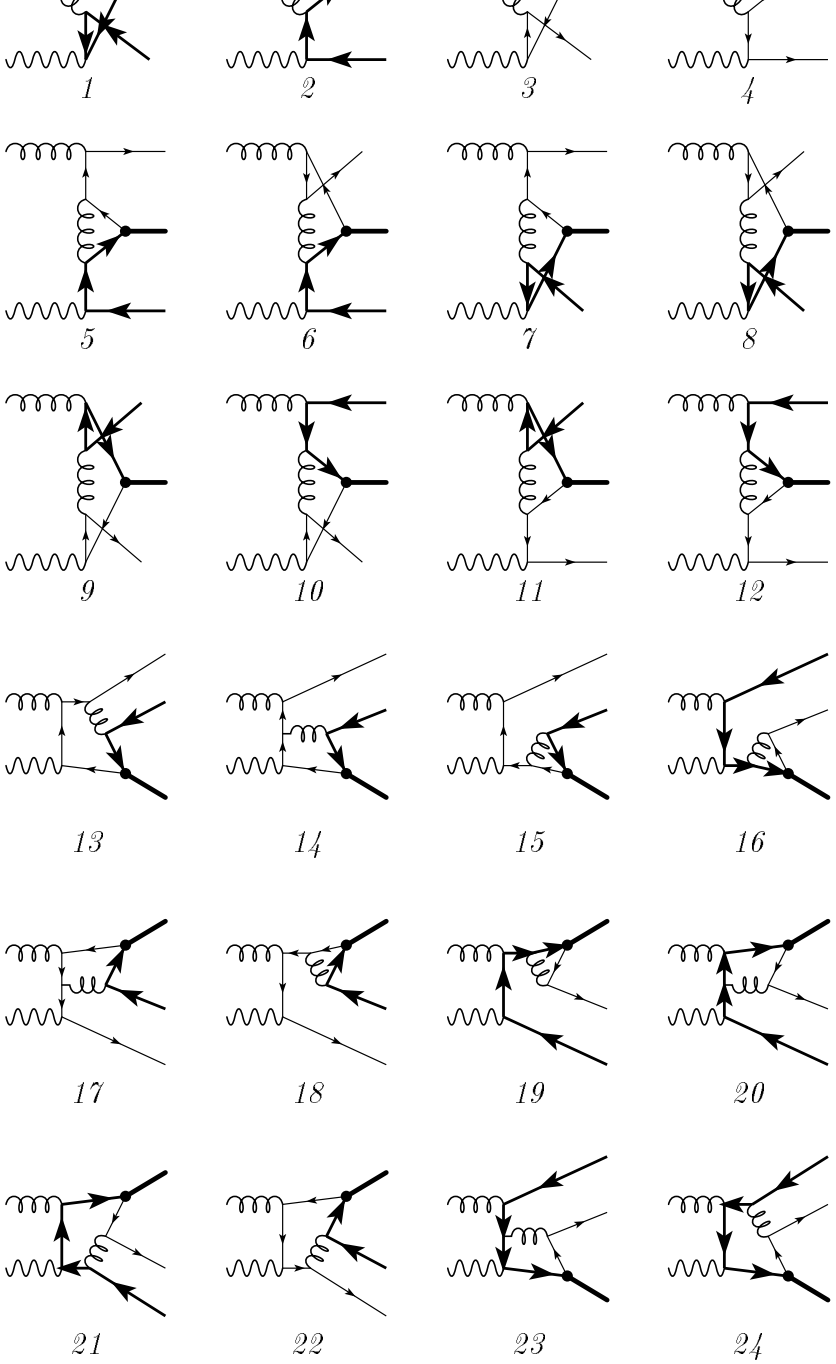

Fig. 1. The leading order QCD diagrams for the $c\bar{q}$-state production in the $g\gamma^*$-interaction.

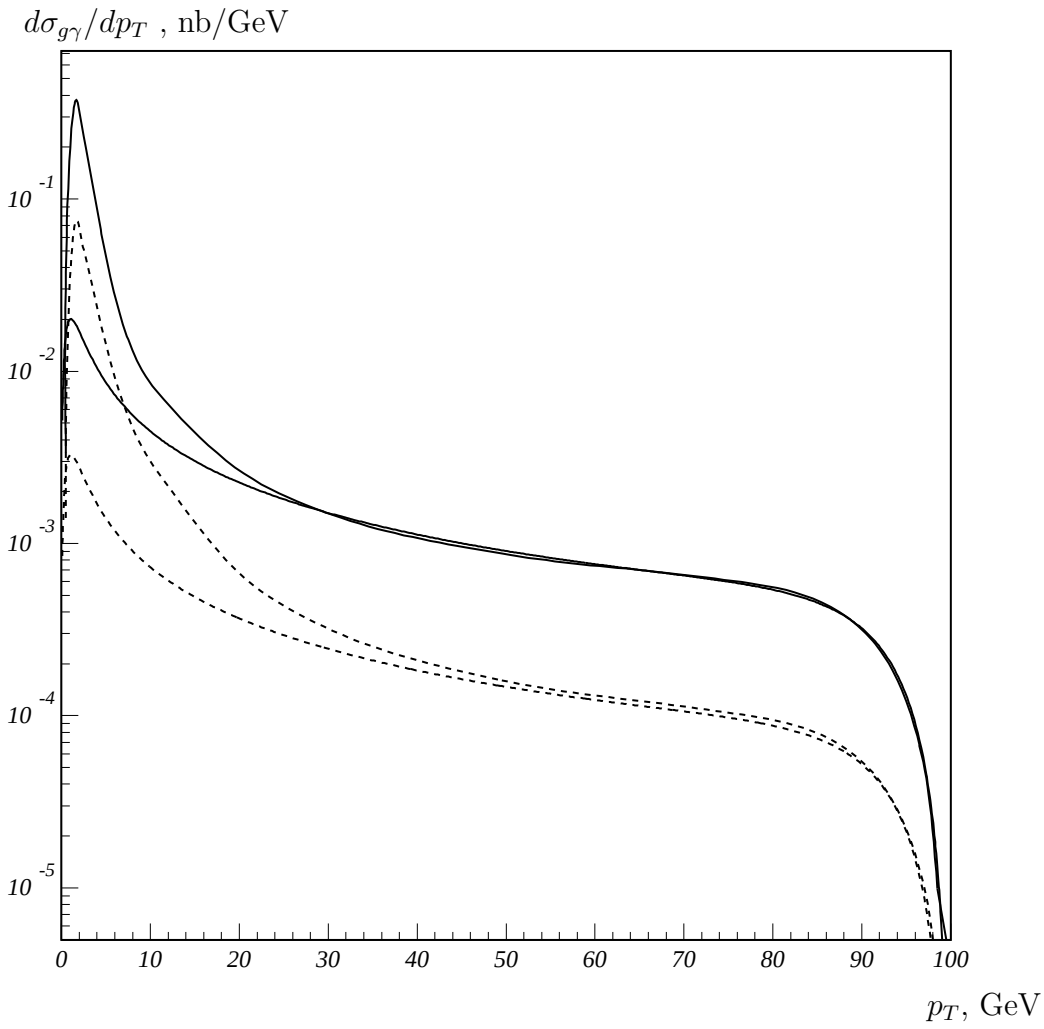

Fig. 2. The D^*-meson production distribution versus p_T calculated in the framework of model under consideration (upper curve) in comparison with the fragmentation model prediction (lower curve) for the $g\gamma$-interaction at 200 GeV.

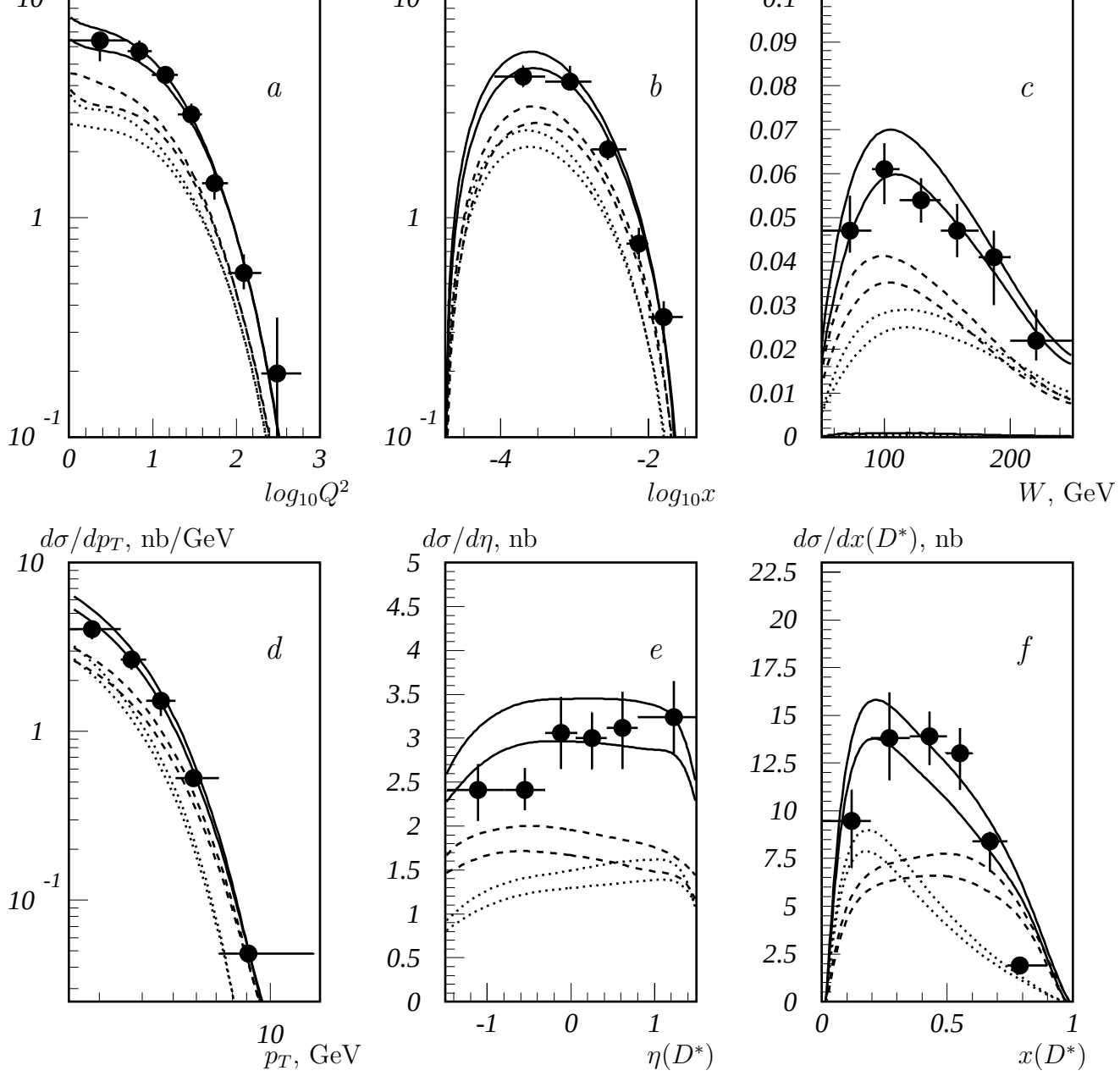

Fig. 3. The differential production cross sections of the D^*-meson for the deep inelastic ep-scattering: over the photon virtuality GeV^2(a), the Bjorken x (b), the invariant mass of the final hadrons (c), the transverse momentum (d), the pseudorapidity (e) and the Feynman variable (f) in comparison with the experimental data of ZEUS Collaboration.

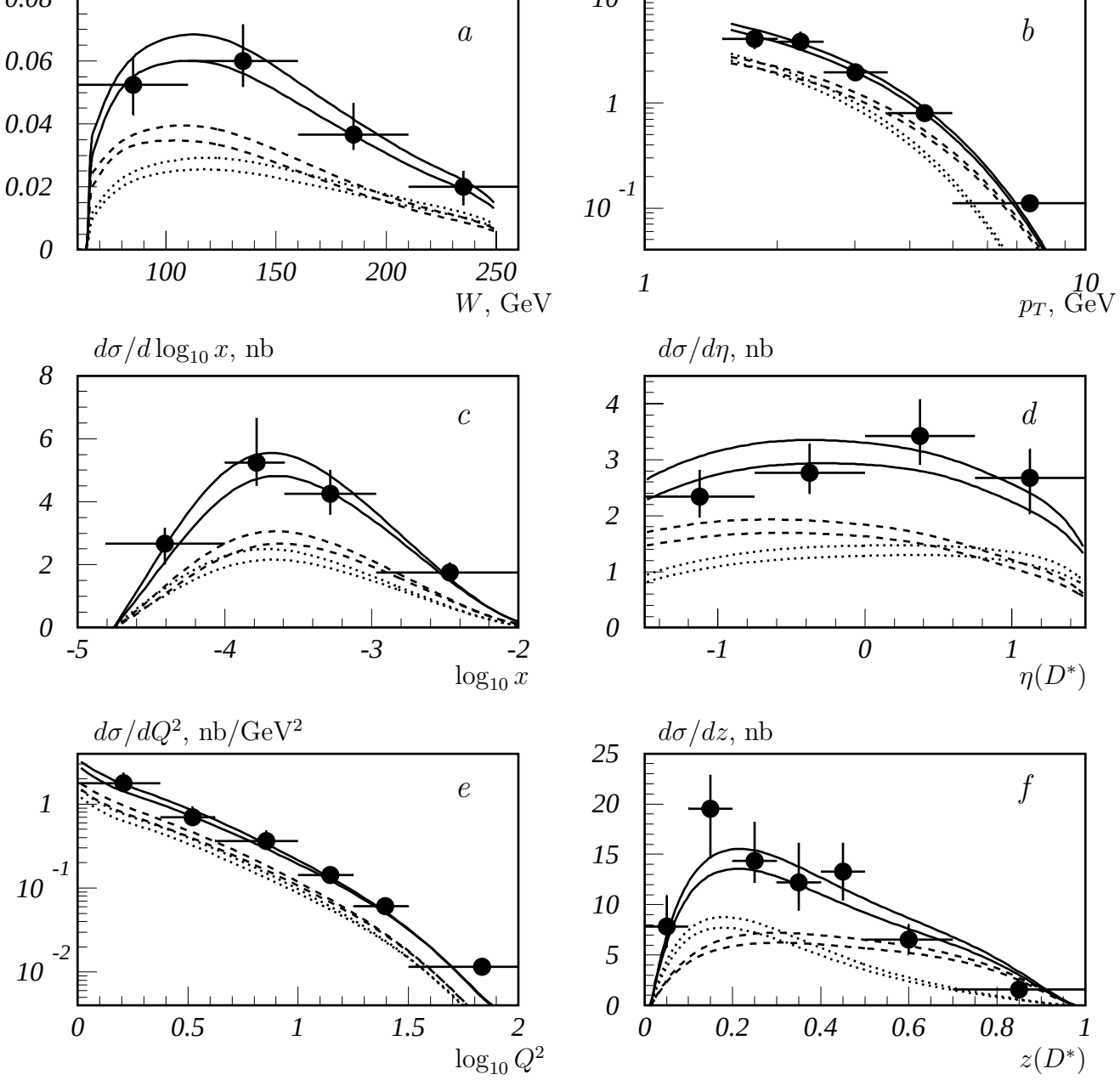

Fig. 4 The differential production cross sections of the D^*-meson for the deep inelastic ep-scattering over the invariant mass of the final hadrons (a), the transverse momentum (b), the Bjorken x (c), the pseudorapidity (d), the photon virtuality GeV^2(e) and $z(D^*)$ in comparison with the experimental data of H1 Collaboration.

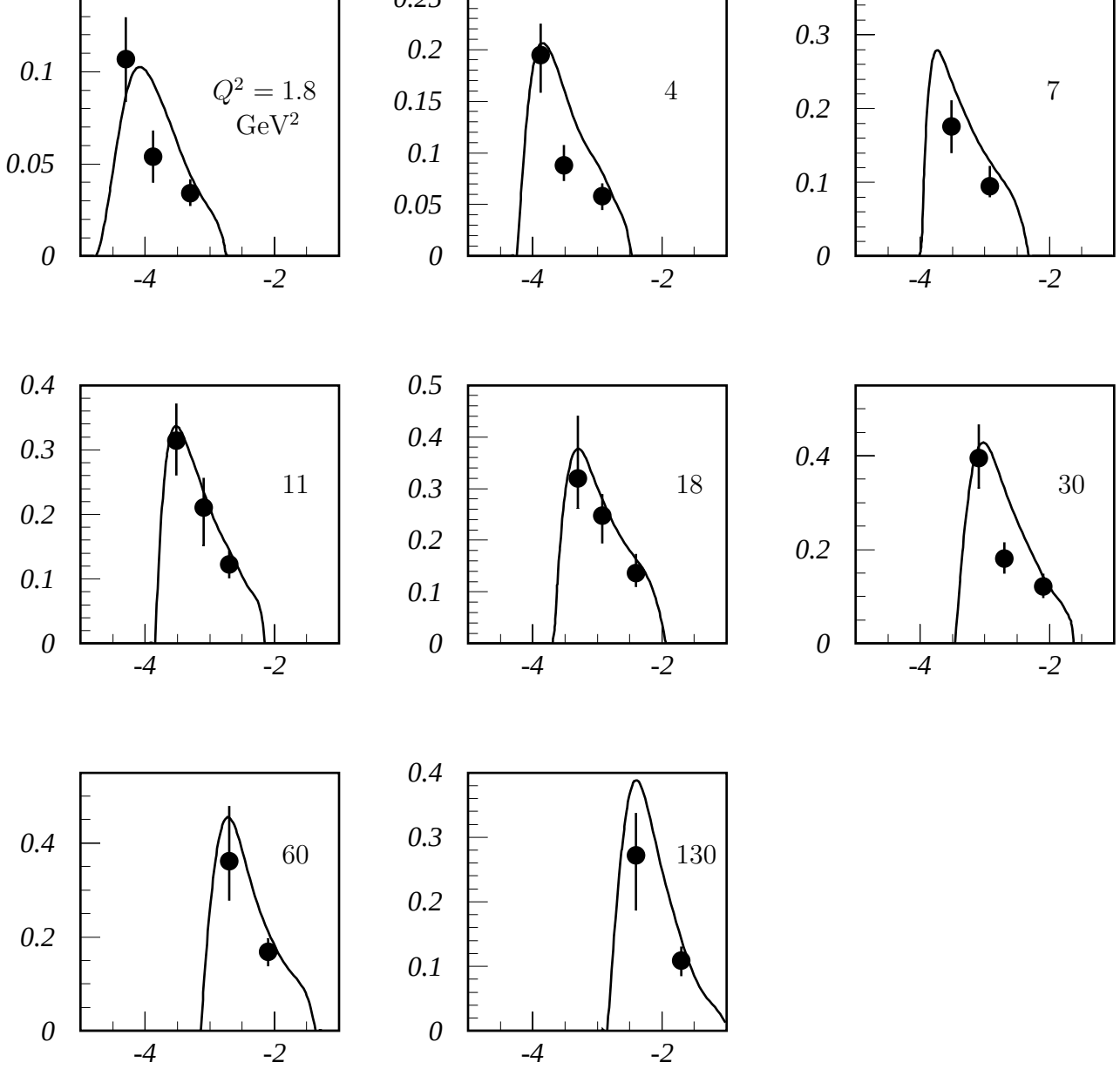

Fig. 5. The experimental values of F_2^c (the ZEUS Collaboration) in comparison with the discussed model predictions.

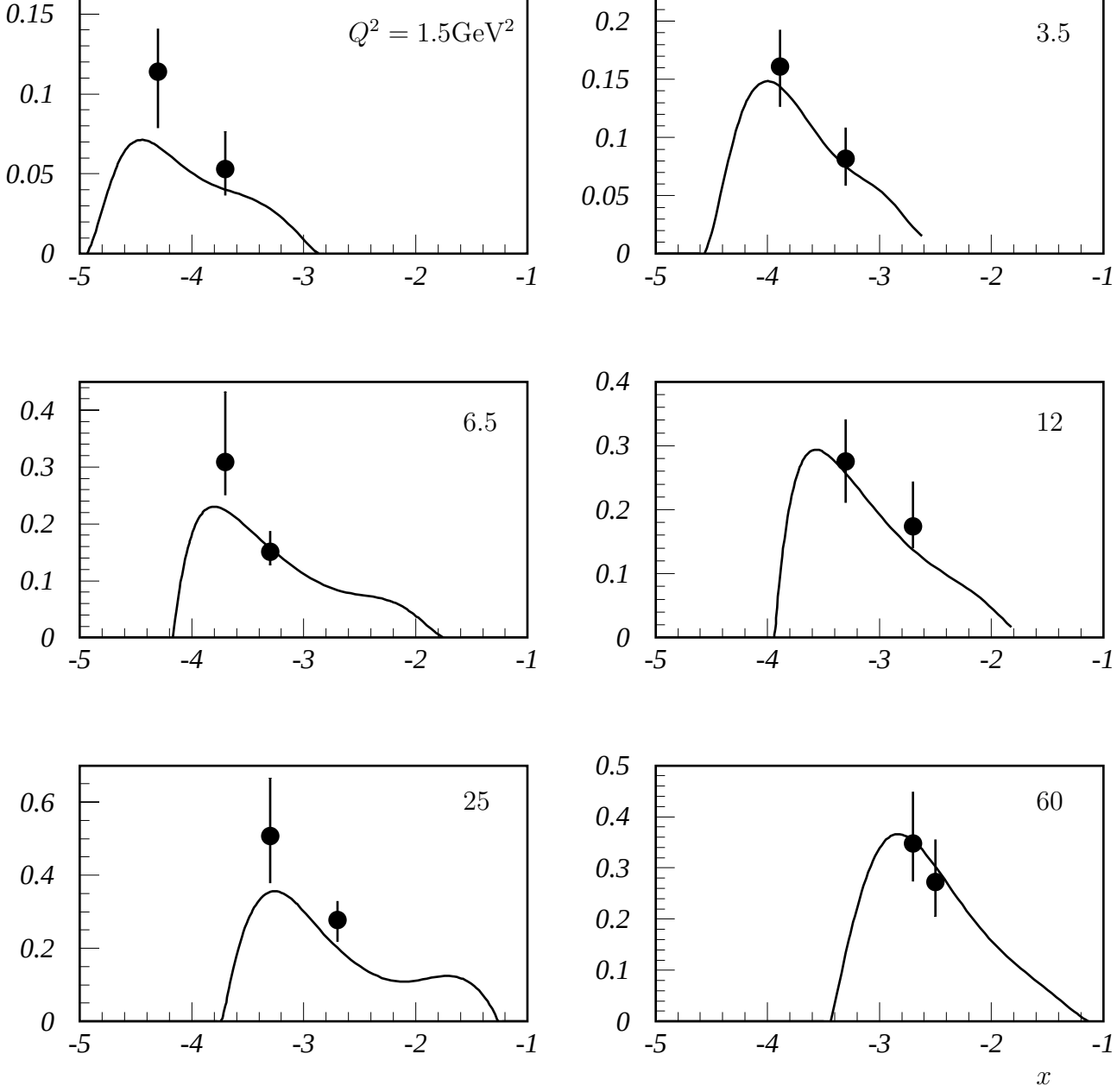

Fig. 6. The experimental values of F_2^c (the H1 Collaboration) in comparison with the discussed model predictions.

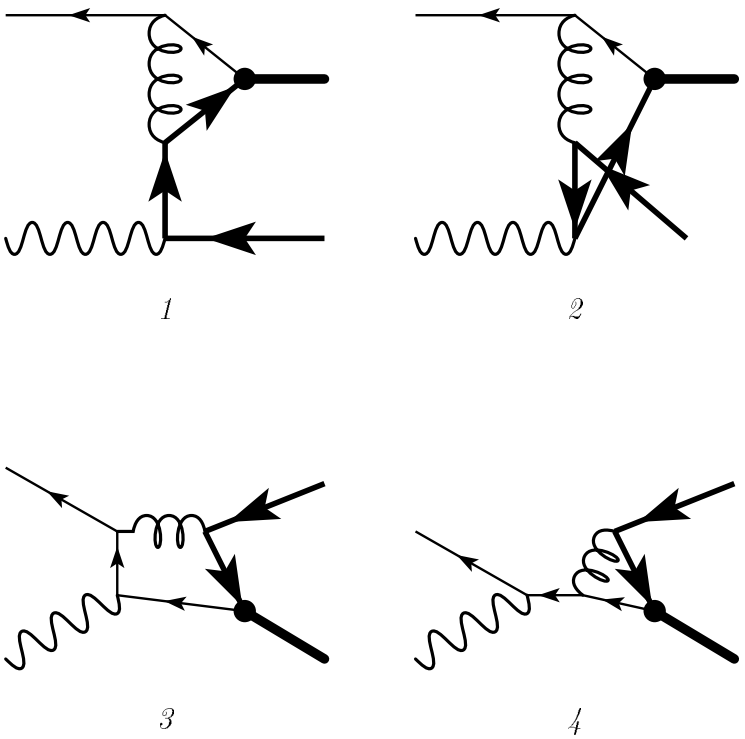

Fig. 7. The QCD leading order diagrams for the $c\bar{q}$-state production in the $\bar{q}\gamma^*$-interaction.

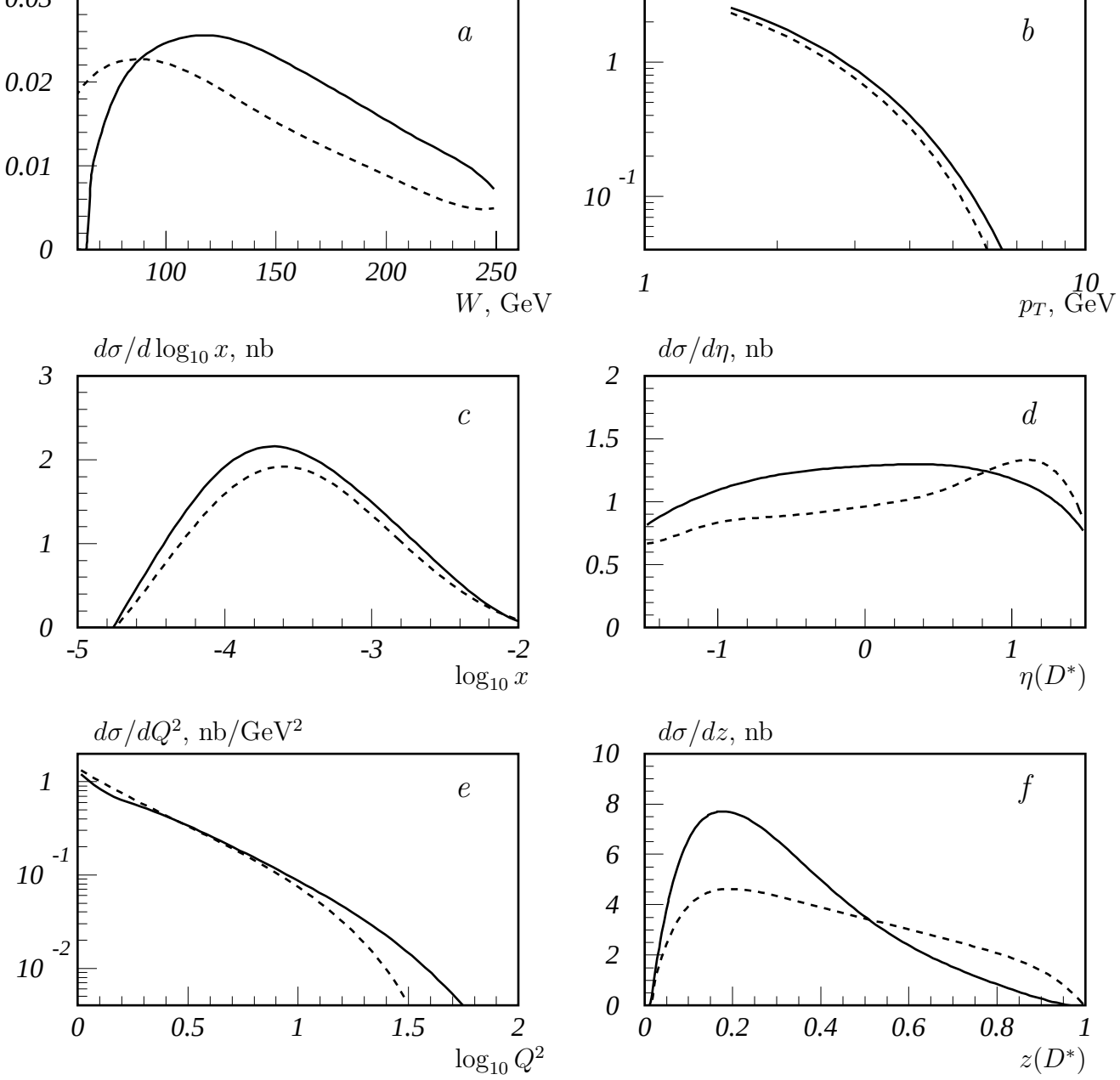

Fig. 8 The singlet $c\bar{q}$-pair production in the $\bar{q}\gamma-$subprocess for the kinematic region of H1 Collaboration in comparison with the octet $c\bar{q}$-pair production in the $g\gamma$-subprocess (the distributions are over the same variables as in Fig. 4).

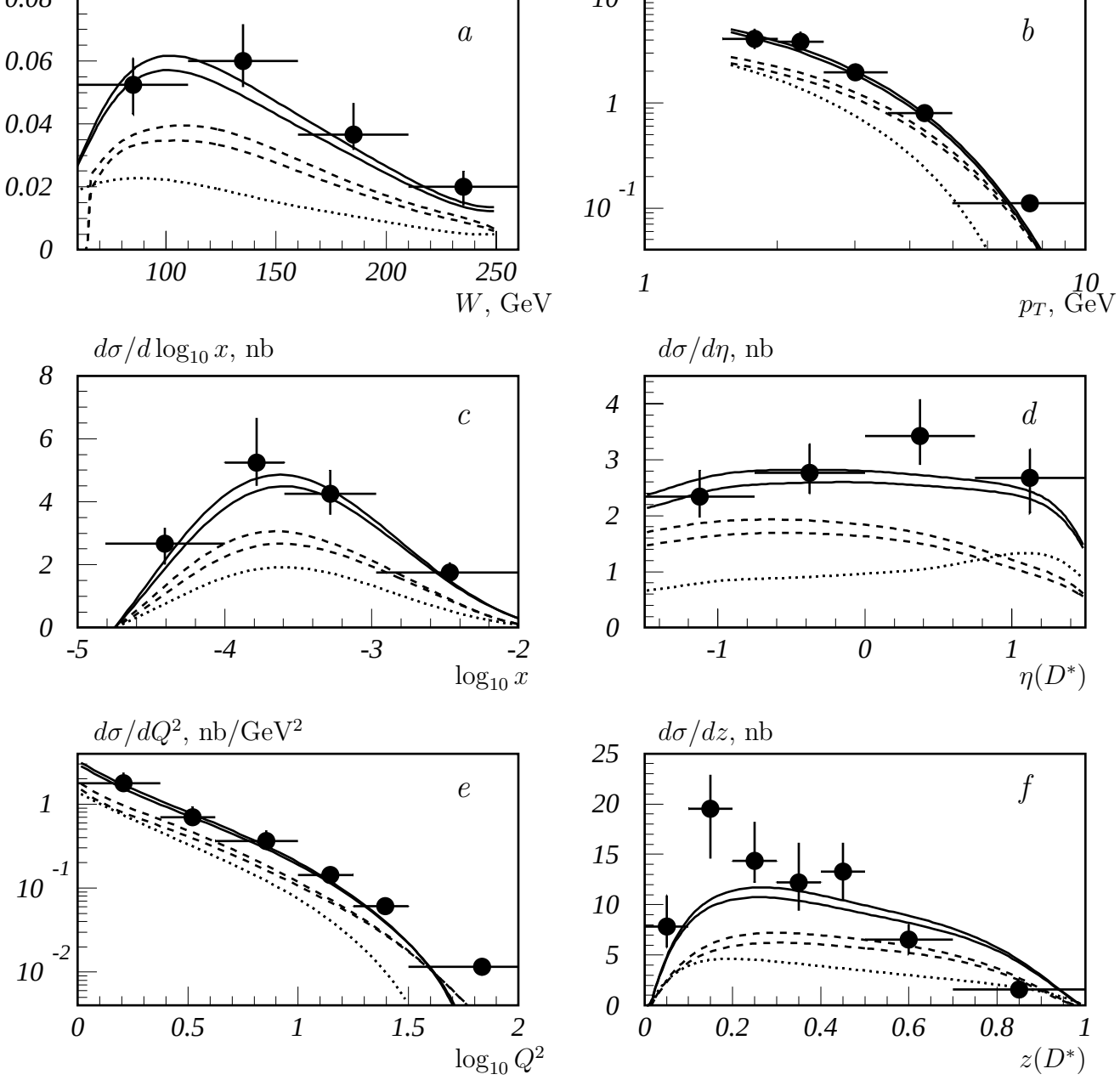

Fig. 9 The sum of singlet $c\bar{q}$-pair production in the $\bar{q}\gamma-$subprocess and the singlet $c\bar{q}$-pair production in the $g\gamma$-subprocess in comparison with the data of H1 Collaboration (the distributions are over the same variables as in Fig. 4).

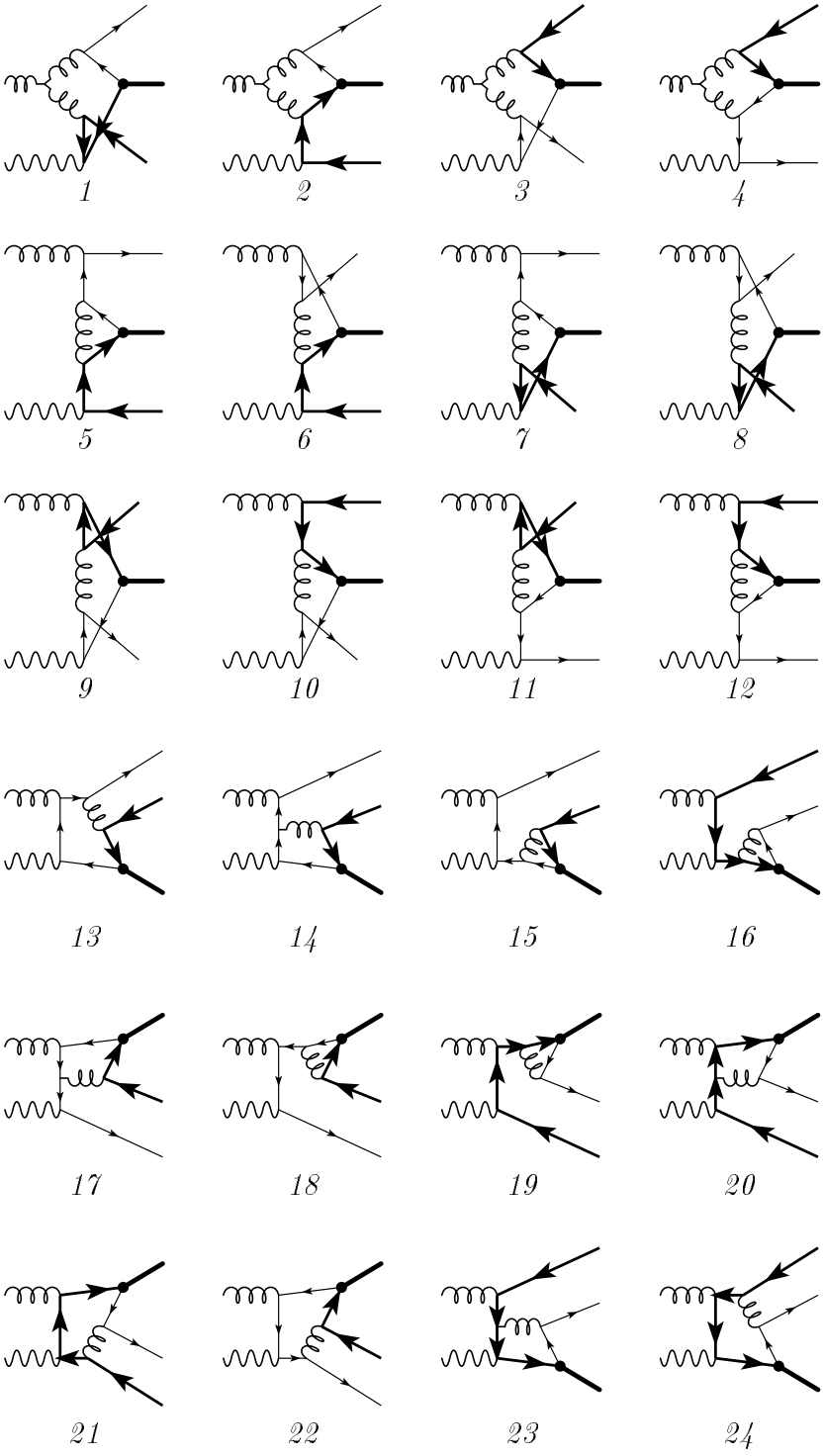
1
2
3
4
5
6
7
8
9
10
11
12
13
14
15
16
17
18
19
20
21
22
23
24

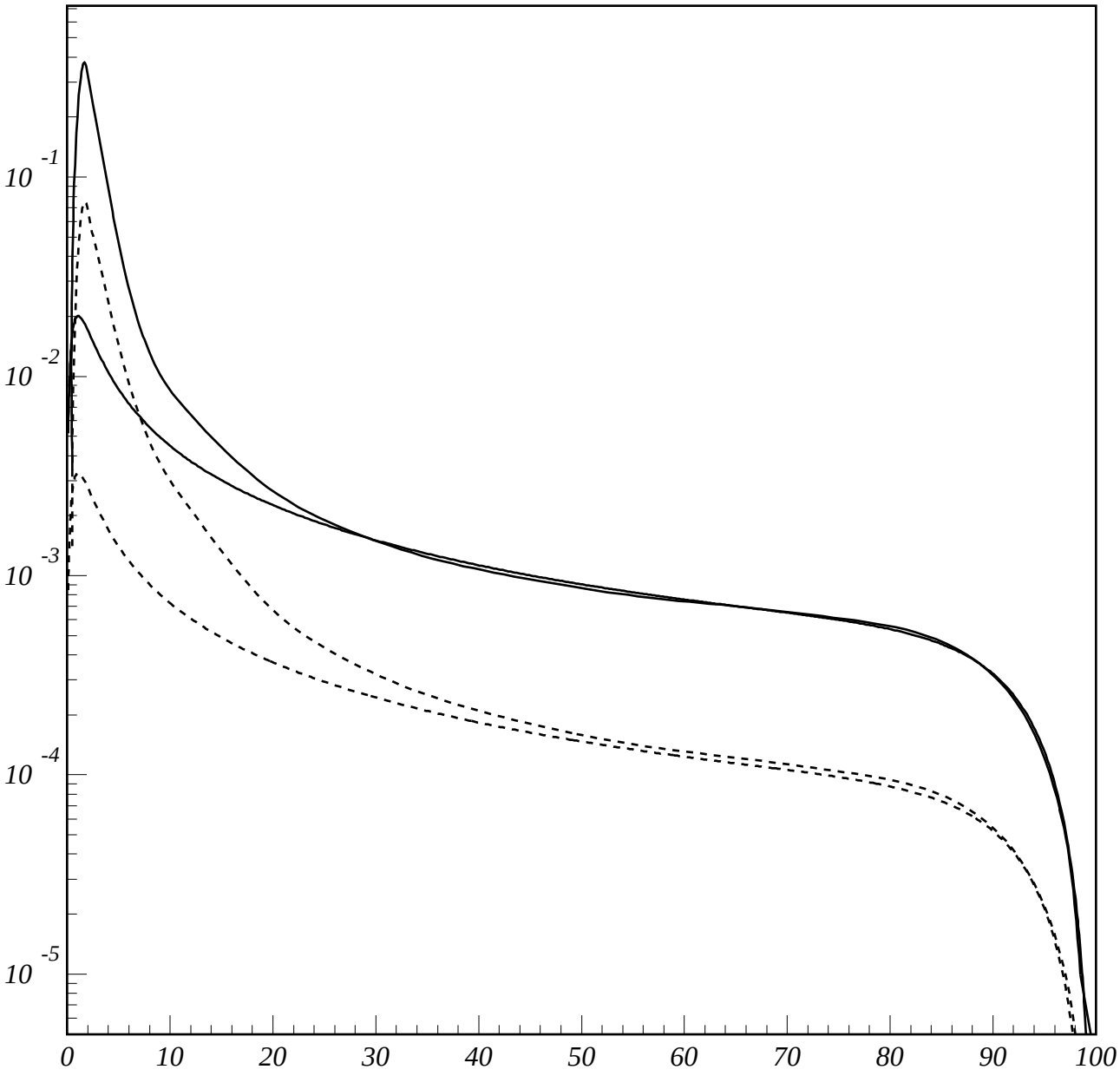
10 -1
10 -2
10 -3
10 -4
10 -5
0
10
20
30
40
50
60
70
80
90
100

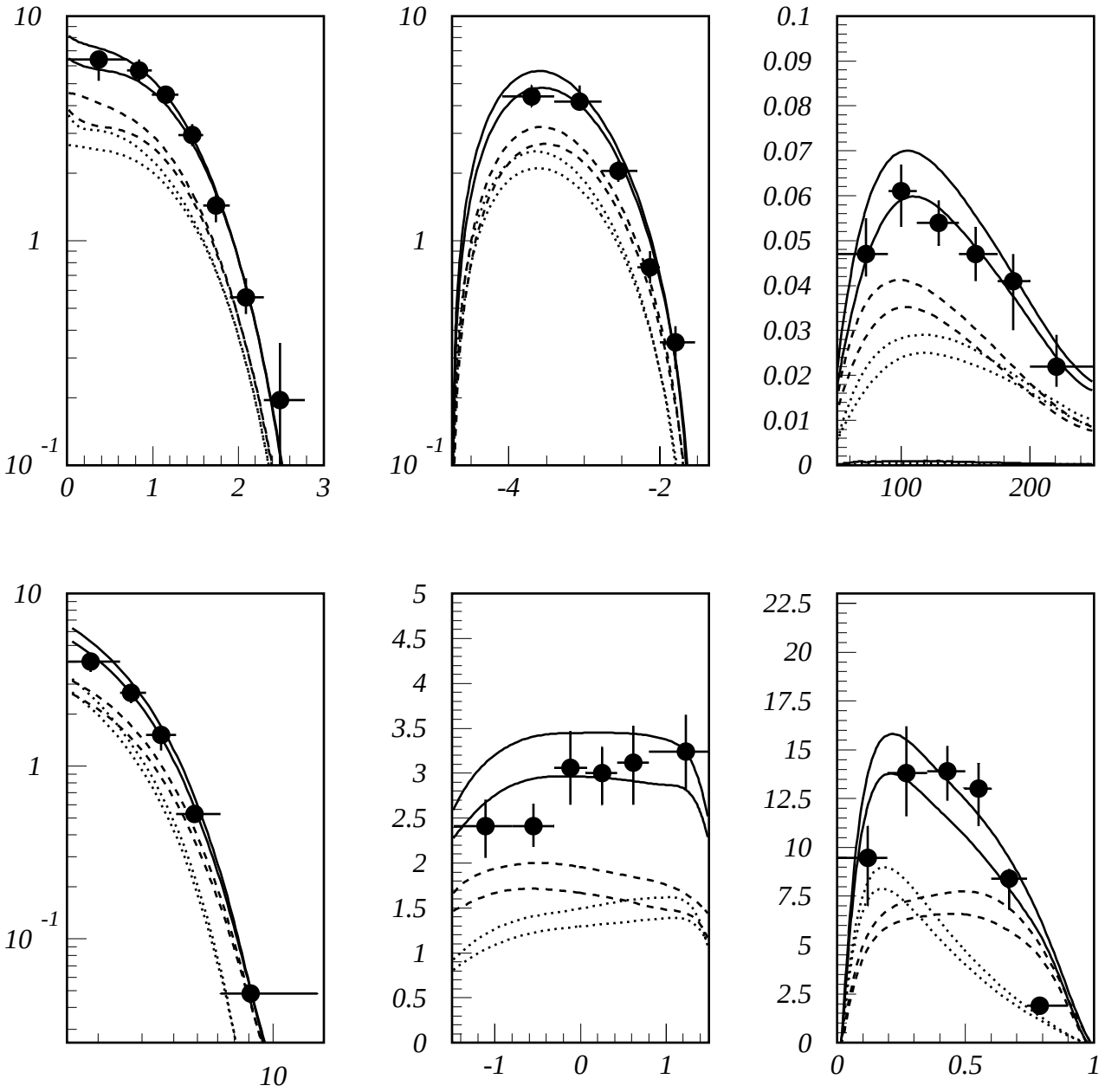
10
1
10 -1
0 1 2 3
10
1
10 -1
-4 -2
0.1
0.09
0.08
0.07
0.06
0.05
0.04
0.03
0.02
0.01
0
100 200
10
1
10 -1
10
5
4.5
4
3.5
3
2.5
2
1.5
1
0.5
0
-1 0 1
22.5
20
17.5
15
12.5
10
7.5
5
2.5
0
0 0.5 1

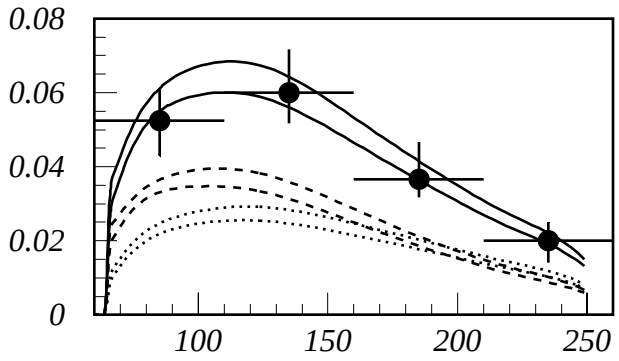
0.08
0.06
0.04
0.02
0
100
150
200
250

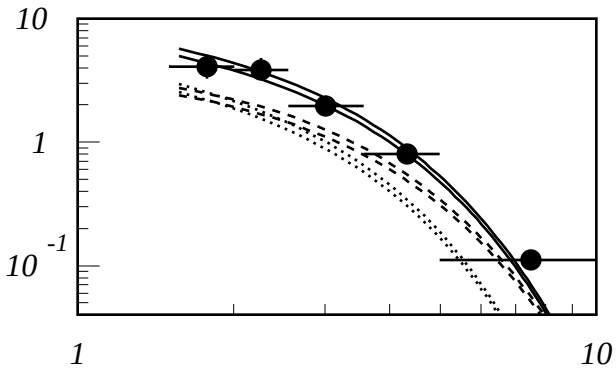
10
1
10 -1
1
10

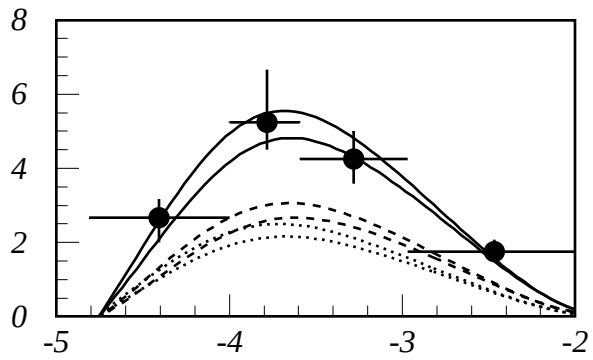
8
6
4
2
0
-5
-4
-3
-2

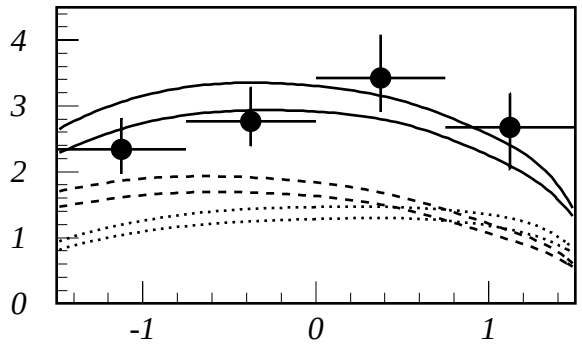
4
3
2
1
0
-1
0
1

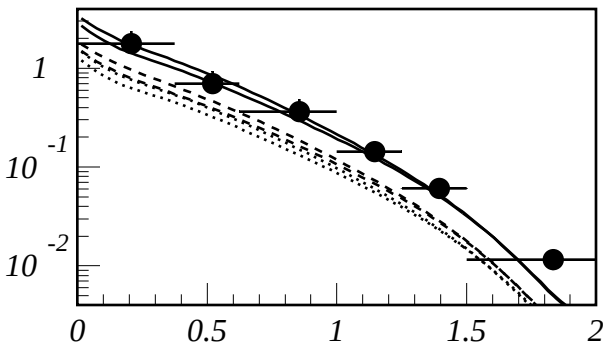
1
10 -1
10 -2
0
0.5
1
1.5
2

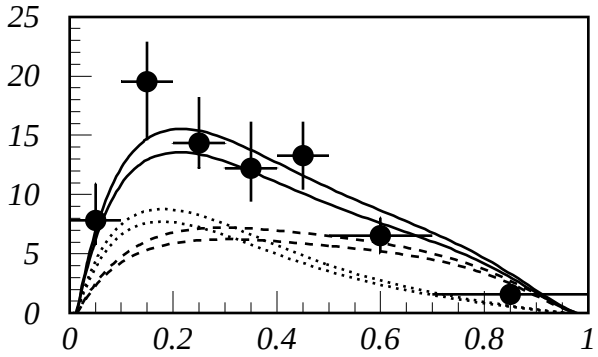
25
20
15
10
5
0
0
0.2
0.4
0.6
0.8
1

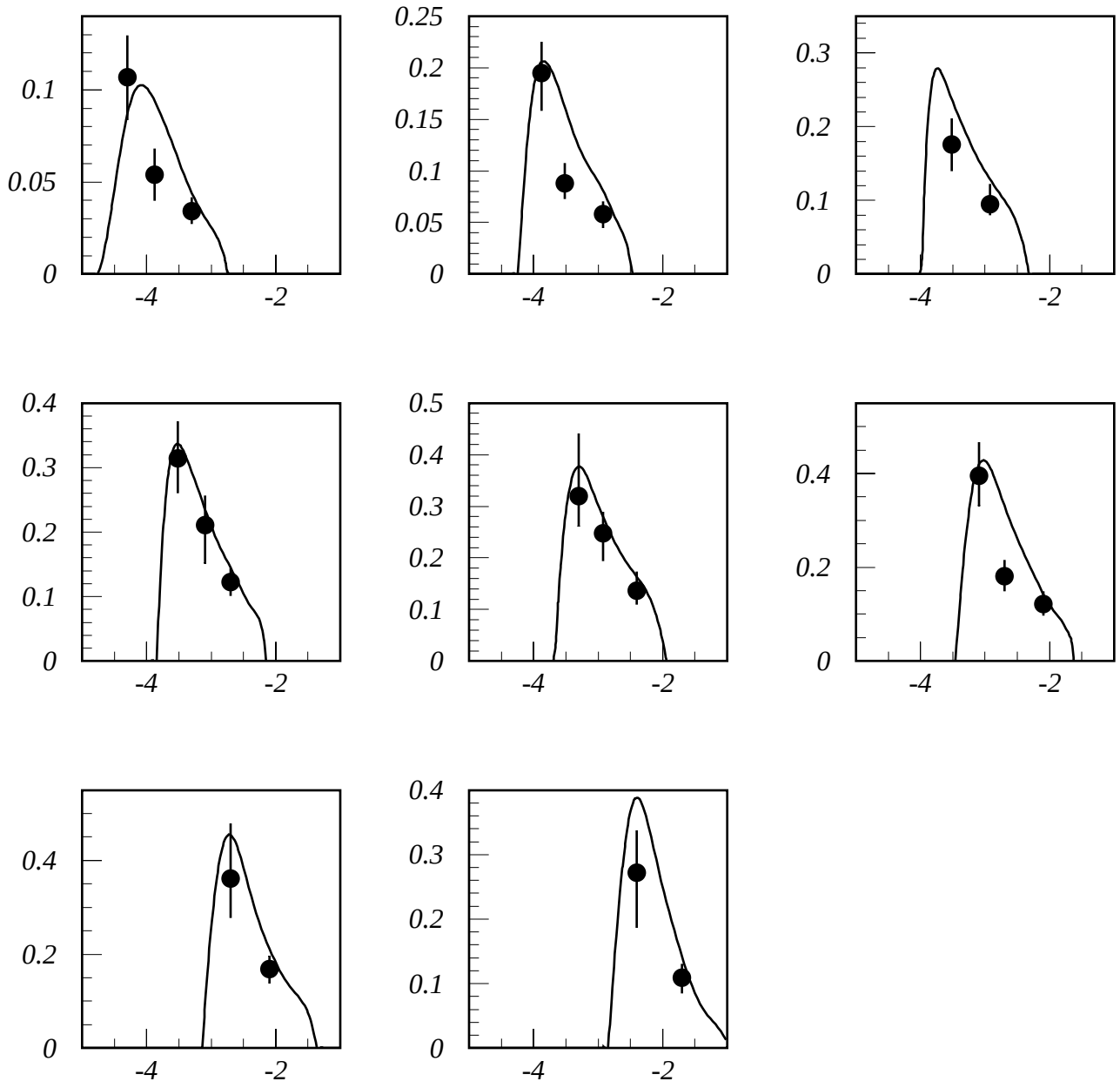
0.1
0.05
0
-4
-2
0.25
0.2
0.15
0.1
0.05
0
-4
-2
0.3
0.2
0.1
0
-4
-2
0.4
0.3
0.2
0.1
0
-4
-2
0.5
0.4
0.3
0.2
0.1
0
-4
-2
0.4
0.2
0
-4
-2
0.4
0.2
0
-4
-2
0.4
0.3
0.2
0.1
0
-4
-2

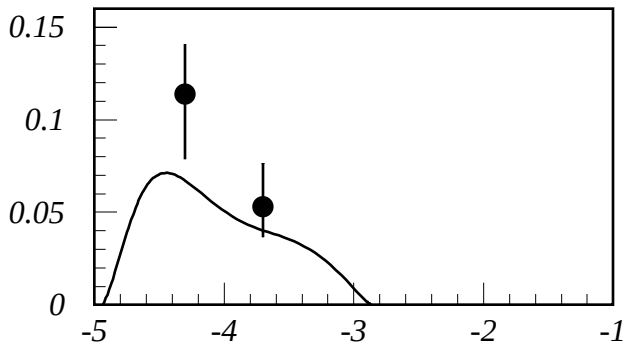
0.15
0.1
0.05
0
-5
-4
-3
-2
-1

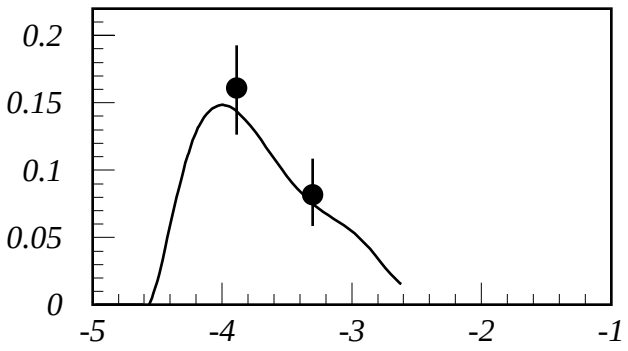
0.2
0.15
0.1
0.05
0
-5
-4
-3
-2
-1

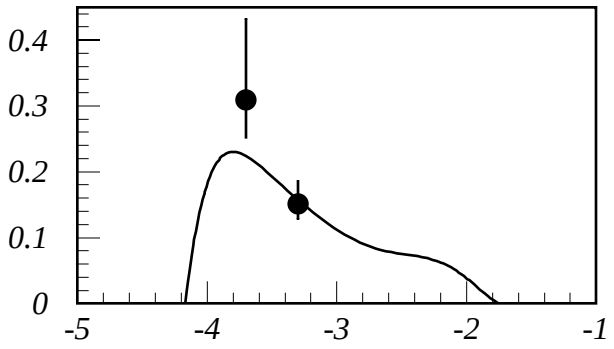
0.4
0.3
0.2
0.1
0
-5
-4
-3
-2
-1

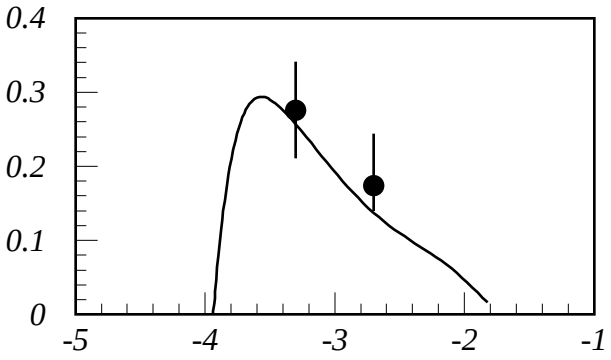
0.4
0.3
0.2
0.1
0
-5
-4
-3
-2
-1

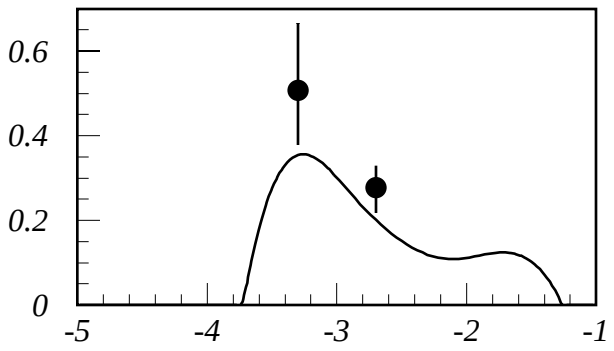
0.6
0.4
0.2
0
-5
-4
-3
-2
-1

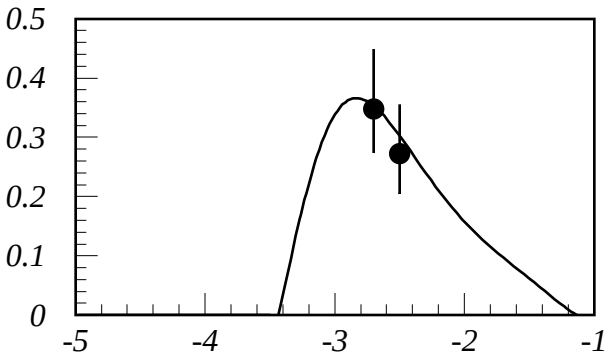
0.5
0.4
0.3
0.2
0.1
0
-5
-4
-3
-2
-1

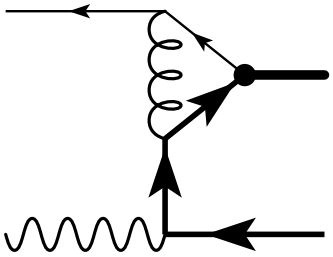

1

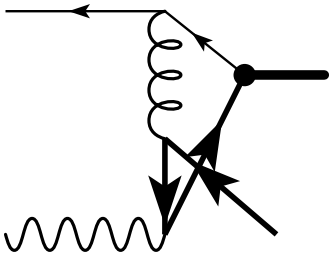

2

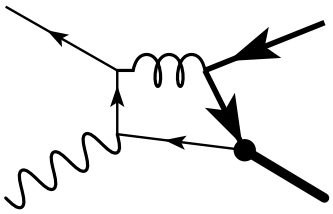

3

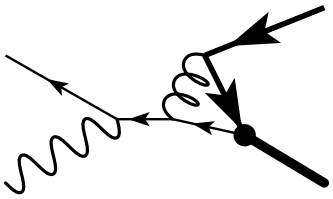

4

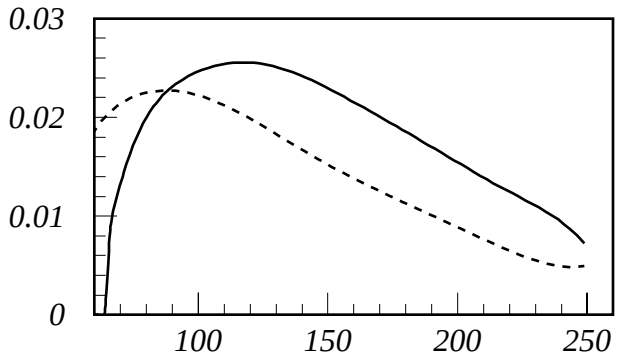
0.03
0.02
0.01
0
100
150
200
250

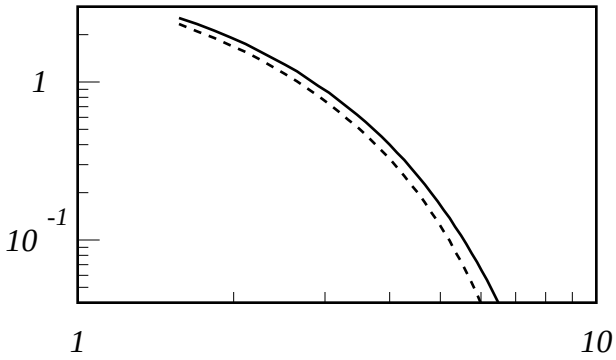
1
10 -1
1
10

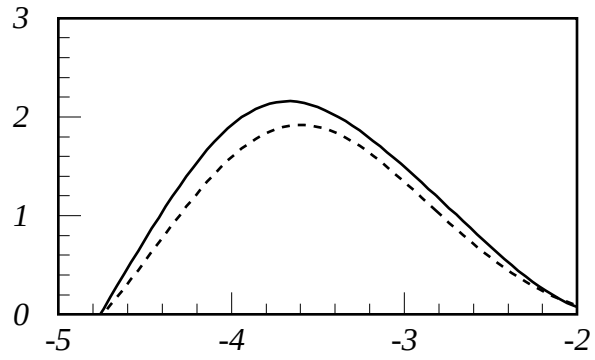
3
2
1
0
-5
-4
-3
-2

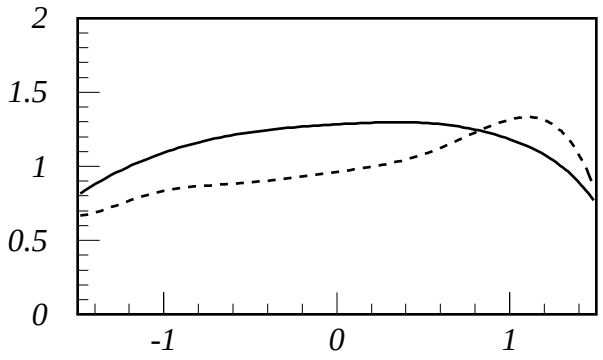
2
1.5
1
0.5
0
-1
0
1

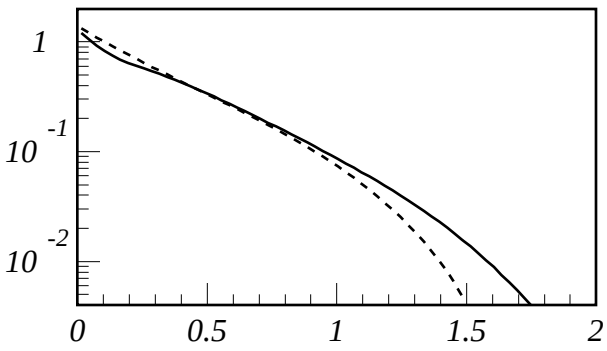
1
10 -1
10 -2
0
0.5
1
1.5
2

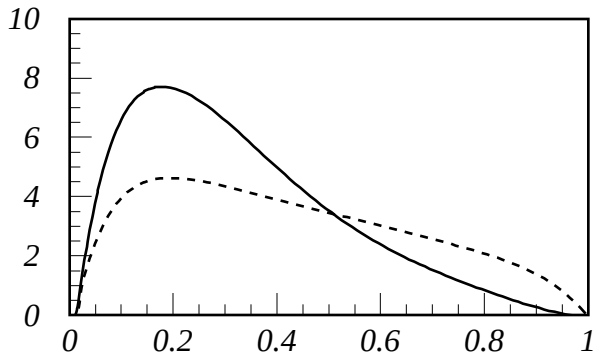
10
8
6
4
2
0
0
0.2
0.4
0.6
0.8
1

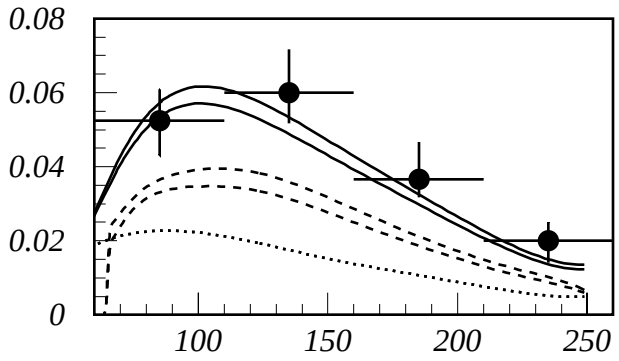
0.08
0.06
0.04
0.02
0
100
150
200
250

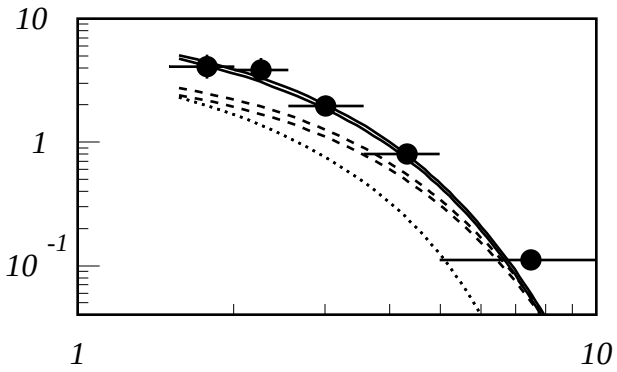
10
1
10 -1
1
10

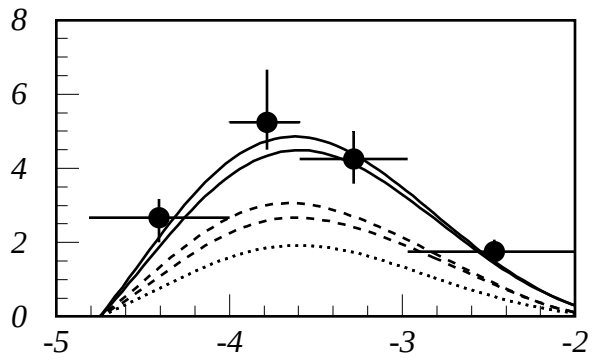
8
6
4
2
0
-5
-4
-3
-2

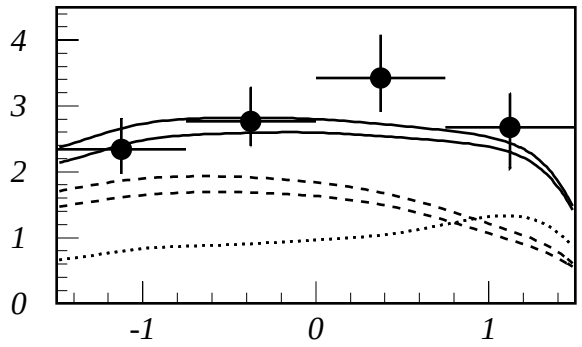
4
3
2
1
0
-1
0
1

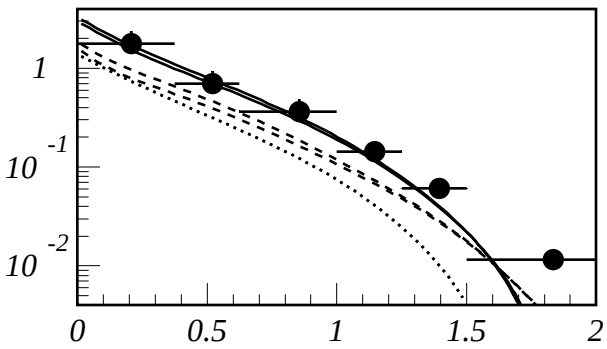
1
10 -1
10 -2
0
0.5
1
1.5
2

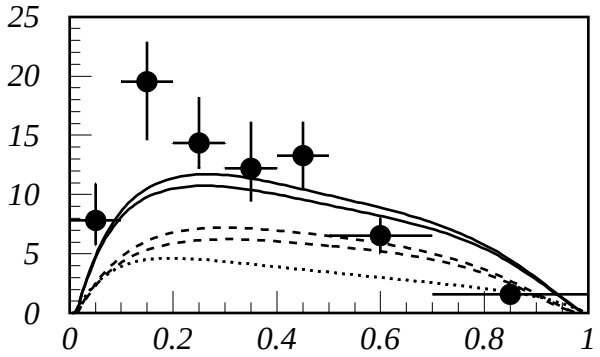
25
20
15
10
5
0
0
0.2
0.4
0.6
0.8
1